This is to certify that the

thesis entitled

Fracture and welding of injection molded polypropylene and short glass fiber reinforced polypropylene

presented by

Feng Cao

has been accepted towards fulfillment of the requirements for

Master degree in Science

Dr. Andre Lee

Major professor

Date 4-5-94

FRACTURE AND WELDING OF INJECTION MOLDED POLYPROPYLENE AND SHORT GLASS FIBER REINFORCED POLYPROPYLENE

By

Feng Cao

A THESIS

Submitted to
Michigan State University
in partial fulfillment of the requirements
for the degree of

MASTER OF SCIENCE

Department of Materials Science and Mechanics

1994

ABSTRACT

FRACTURE AND WELDING OF INJECTION MOLDED POLYPROPYLENE AND SHORT GLASS FIBRE REINFORCED POLYPROPYLENE

By

Feng Cao

The fracture toughness, K_c, was found to increase with fibre content for notched compact tention specimens in short glass fibre reinforced polypropylene (GF-PP) at low temperature. When fibre content is low, (from 5% to 10% w/o, weight percent), K_c increase quickly and the toughening mechanism is proposed to be that of crack pinning. However, the fracture toughness increases at a slower rate when fibre content is above 10% w/o. In this case, the toughening mechanism is best explained by the model of crack deflection. Furthermore, when the fibers are arranged transverse to the notch, we observed an higher higher K_c value. In the welding of PP to GF-PP, significant interfacial strength is developed at temperature higer than 167 ^oC. The welding time affect not only the strength but also the failure behavior of the joints. The failure occurred all through the interface to a small part in the center of the interface as welding time increased. It was found out that the strength of PP to GF-PP and GF-PP to GF-PP butt-joints could reach ultimately reach that of the bulk PP.

To my parents and to Jie

ACKNOWLEDGMENTS

Thanks to my advisor, Prof. Andre Lee for his support, patience and guidance. Thanks to Himont company for providing the experimental material, and to Prof. James Lucas for using the Instron machine in his laboratory and for his many helpful suggestions.

TABLE OF CONTENTS

List of Tables

List of Figures

CHAPTER 1

INTRODUCTION

Generally speaking, fiber reinforced thermoplastics have better mechanical properties than the unreinforced polymers do, such as higher tensile strength, yield strength, elastic modulus and relative temperature resistance. Fibre increases the strength and stiffness, but decreases the toughness for some thermoplastics. For example, polypropylene (PP) is toughner than fibre reinforced polypropylene at room temperature, however, this is not the case when temperature drops below the glass transition temperature of PP. It is undoubtable that the increment of toughness in glass fiber reinforced polypropylene (GF-PP) resulted from the intervening of fibres with the matrix. The basic principle increasing the toughness of resin-based composites lies in the introduction of various energy-absorbing processes such as filler (particulate or fibre) deformation, debonding of the interface, fiber pull-out, homogeneous and localized plastic deformation of the matrix, and multiple cracking. The typical theoretical models which have been proposed to describe the toughening mechanisms including crack pining (Lange, 1970), crack deflection (Farber and Evans, 1983) and crack blunting (Owen, 1979).

The purpose of this study is to investigate the effect of fiber content on the toughening mechanisms in short glass fiber reinforced PP at low temperature. In addition, the arrangement of fibres in the thickness of injection molded GF-PP plaques affect the fracture toughness is taken into consideration.

Another separate subject that is the application of GF-PP is the welding of GF-PP parts both for PP to GF-PP and GF-PP to GF-PP. Short glass fiber reinforced PP is widely used in the industries of automobile and domestic appliances. A good joint is very important to the integrity of structure as a whole.

The joining of plastics and composites could be dated back to the original study of amorphous polymers. When two samples of the same amorphous polymer are brought into contact at a temperature above the glass transition temperature, the interfacial surface gradually disappear. It is reflected by the increase of interfacial strength until. At long contact times, it is possible to achieve the property of the bulk polymer. At this point the junction surface has become indistinguishable from any other surface that might be located with in the bulk material which is described as compeletly "healed" (Voyutskii, 1963). Effect of time, temperature, molecular weight of polymer on welding or healing of amorphous polymers has been an area of considerable activity, both experimentally (Jud et al., 1981 and Wool et al. 1982) and theoretically (de Gennes, 1980, Prager et al. 1980). Theoretical models have combined the reptation theory of self-diffusion in polymer melts with molecular criteria and with crossing density criteria, describing an increase in interfacial strength as interdiffusion progresses to predict the time dependence of the healing process. However, There is not a successful model to predict the interfacial strength and fracture energy for welding semi-crystalline polymers and their composites. Individual study of the strength and interface of semi-crystalline polymers to their composite joints is very important.

The joint of PP to PP is very easy to approach by various welding methods, such as hot tool, vibration (Stokes, 1988), but very few reportes on the studies of welding PP to GF-PP and GF-PP to GF-PP are available in the literature. In this study, the effect of the processing time and temperature on the strength development of welding PP to short glass fibre reinforced PP was carried out. The fibres in the weld region involved in the failure of the welded specimen was taken into consideration. Finally, the mechanical properties of GF-PP to GF-PP joints were tested and analyzed.

CHAPTER 2

Toughening Mechanisms of Short Glass Fiber Reinforced Polypropylene

2.1 Introduction

The important parameters determining the mechanical properties of resin-based composites are the volume fraction of the filler, which may be particulates or fibers, its particle size or fibre aspect ratio, its modulus and strength, the fiber-matrix adhesive, and the toughness of the matrix.

Short fiber reinforced polypropylene has been widely used in automobile and domestic structures. At room temperature, the matrix toughness plays an important role in determining the mechanical properties of short fiber reinforced polypropylene (GF-PP) (Gupta et al. 1983). Gupta et al. studied the energy-absorbing mechanisms during fracture in glass fiber reinforced PP and suggested that the total work of fracture included contributions from the debonding of the interface, the sliding or pull-out of fibers, and the plastic deformation of matrix. They reckoned that the contribution from matrix plasticity, either through homogenous deformation of the matrix or from localized deformation around the fiber ends, was dominant.

When the testing temperature drops below glass transition temperature of PP, the matrix in short fiber reinforced PP will become brittle. In this case, the toughening mechanisms and the main energy-absorbing mechanisms during fracture may differ from those at room temperature. In addition, injection molding introduces the different arrangement of fibers across the thickness of molded plaques of short fiber reinforced thermoplastics. This gives rise to various fiber-related failure mechanisms (Friedrich, 1989) which has effect on the toughening result.

The objective of present study is to investigate the effect of fiber content on the toughening mechanisms of short glass fiber reinforced PP at low temperature.The fiber related failures in GF-PP are determined from the fracture surfaces. The effect of various arrangement of fibres in GF-PP are analyzed.

2.2. Background

2.2.1. Toughening Mechanisms in Particle Filled Resin-Based Composites

The basic principle increasing the toughness of resin-based composites lies in the introduction of various energy-absorbing processes such as filler (particulate or fiber) deformation, debonding of the interface, fibre pull-out, homogeneous and localized plastic deformation of the matrix, and multiple cracking. The typical theoretical models which have been proposed, including, crack pining, crack deflection and crack blunting.

The crack pining mechanism was suggested and modified by Lange (Lange, 1970), Lange and Radford (Lange and Radford, 1971) and Evans (Evans, 1972) in the study of particulate reinforced composites. The increase in toughness of filled composites was explained in terms of a crack pining mechanism in that the rigid particles act as obstacles and force the crack to bow as shown in Figure 1. This model is similar to the interaction between dislocation and dispersed particles in the plastic deformation of metals. The interaction between the crack and the reinforced particles occurs during crack propagation in the case of good filler-matrix adhesion. Therefore, the hindered crack can only bow out between the well-bonded particles, forming secondary cracks and breaks away from pining positions when it attains a radius of (D/2), where D is the interparticle spacing. The toughening effect depends on the interparticle spacing, D, and the effective crack line tension, T. The maximum toughening effect can be expressed as

$$G_{comp} = G_{matrix} + \frac{T}{D} \qquad (1)$$

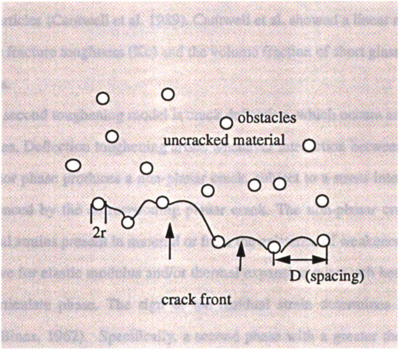

Figure 1: Schematic representation of the process of crack pinning.

where G_{comp} and G_{matrix} are the fracture energies of the composite and matrix respectively. The contribution to T originates from dissipation processes, such as debonding of the filler-matrix interfaces, local plastic deformation near the interface etc. Although these results have been obtained primarily through the study of spherical particle reinforced resin composites, for example, alumina trihydrate epoxy (Lange and Radford, 1971) and glass beads-epoxy resin (Kinloch, et al. 1989), in principle the, they may be adequate to describe the behavior of other types of composites filled by non-spherical particles (Cantwell et al. 1989). Cantwell et al. showed a linear relationship exits between the fracture toughness (Kc) and the volume fraction of short glass fibre reinforced epoxy resins.

The second toughening model is crack deflection, which occurs around the second filler particles. Deflection toughening arises whenever interaction between the crack front and the minor phase produces a non-planar crack, subject to a stress intensity lower than that experienced by the corresponding planar crack. The non-planar crack arises either from residual strains present in material or from the existence of weakened interfaces. The former derive for elastic modulus and/or thermal expansion mismatch between the matrix and the particulate phase. The sign of the residual strain determines the direction of deflecting (Binns, 1962). Specifically, a second phase with a greater thermal expansion coefficient or elastic modulus than that of the matrix, produces tangential tensile strains, causing the crack to deflect toward the particle. When a crack approaches or intercepts a second phase particle or other kind of filler, it will tilt at an angle, θ, out of its original plane and subsequently twist at an angle, ϕ, as shown in Figure 2 (a) and (b) respectively. The initial tilt angle depends upon the orientation and position of the particle and the matrix. Farber and Evans (Farber and Evans, 1983) based upon a fracture mechanics approach to predict the toughness of reinforced composites, both theoretically and experimentally. They pointed out that the increase in toughness depends much upon the shape and volume fraction of the filler, but is invariant with size of the filler, according to the

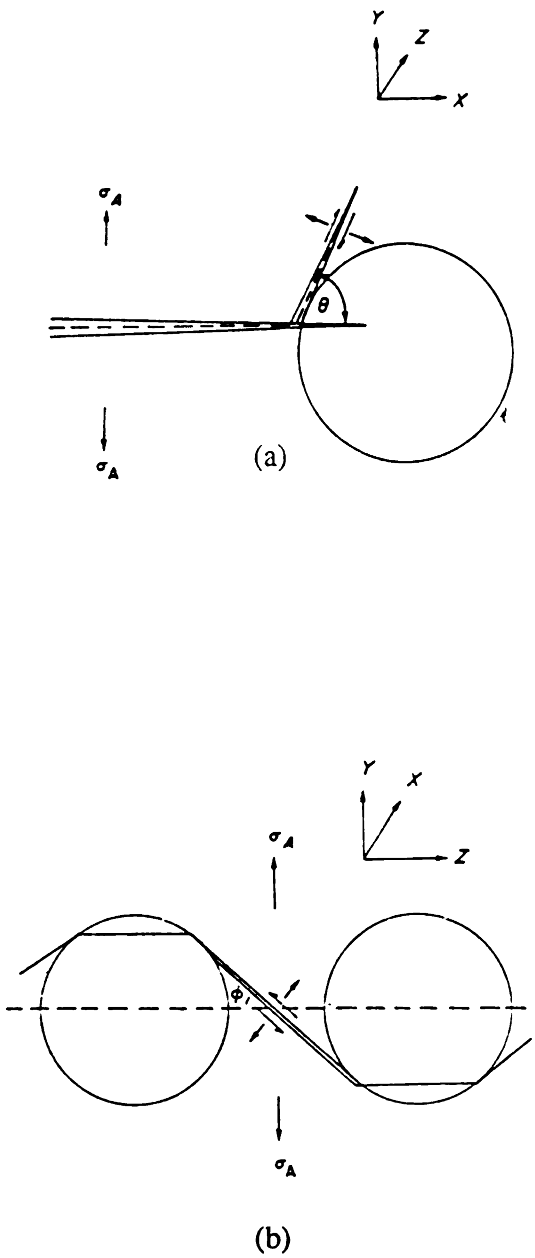

Figure 2: Schematics of typical crack deflection: (a) tilt, and (b) twist of the crack front

mathematical model. The most effective morphology for deflecting propagation cracks is the rod of high aspect ratio of which short glass fibre is an example. Less effective in toughening are disc-shaped particles and spheres. The ideal second phase, in addition to maintaining chemical compatibility, should be present in amounts of 10 to 20 % percent by volume. Greater amounts may diminish the increase in toughness due to overlapping particles.

In the case of poor filler-matrix adhesion, the toughening mechanism through crack tip blunting is important. Evidence of decohesion of the particles ahead of the crack tip has been given by Owen (Owen, 1979) in a study of the fracture properties of glass bead-filled resin. Early debonding leads to blunting of the crack tip, by which the stress intensity factor, Kc, near the crack tip reduces considerably. It has been observed in some composites with poor filler-matrix adhesion that the crack tends to propagate in an unstable stick-slip manner. When unstable propagation occurs, the load-displacement curve has a characteristic sawtooth shape (Lin and Lai, 1993). It appears that the unstable stick-slip propagation is probably due to repeated crack initiations and arrests due to the crack tip blunting.

Except for the above three typical toughening mechanisms in short fiber reinforced composites, fiber pull-out and deformation of matrix and fibers are very important energy consuming mechanisms which intervene during crack propagations (Gupta et al., 1990). However, it is very difficult to predict their contribution to the total fracture energy of fiber pull-out by qualitative study because it is a dynamic process during the failure of composite (Cantwell et al. 1989). The crack pinning, crack deflection, crack blunting and other energy absorbing mechanisms such as fiber pull-out deformation of matrix and fibers, debonding of filler/matrix could occur simultaneously or separately during fracture of reinforced composites by particulates and fibers or other kinds of fillers (Faber and Evans, 1983)

2.2.2 Linear Elastic Fracture Mechanics

The subject of fracture mechanics was developed from the basic concept of Griffith (Griffth, 1920) dealing with brittle materials. The strength of a brittle material is governed by small defects that act as stress concentrators, in accordance with the equation:

$$\sigma_F = \left(\frac{2\gamma E}{\pi c}\right)^{\frac{1}{2}} \qquad (2)$$

where:

σ_F - tensile strength

E - tensile modulus

γ - fracture surface energy

c - the length of intrinsic defect

Figure 3 is a typical diagram presenting a realistic crack in an infinite specimen to calculate the crack opening mode stress intensity factor. The result was concluded as:

$$K_I \propto Y\sigma\sqrt{\pi a} \qquad (3)$$

and the strain energy release rate for the opening mode is

$$G_I = \frac{K_I^2}{E} \qquad (4)$$

It is assumed that a crack will propagate when K_I reaches a critical value, K_{Ic}, which is specific for each material. G_{Ic}, is respectively, is the critical strain energy release rate. K_c, the critical value of stress field intensity factor, is derived from the tensile strength of a sharply notched specimen by a transformation based on the specimen geometry. It is a relatively simple physical quantity and the related G_c is even simpler and

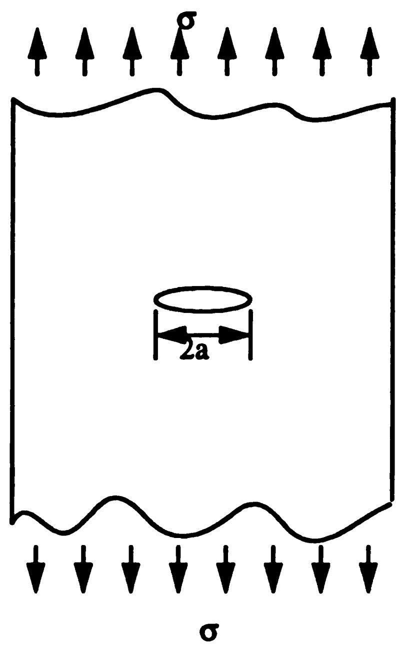

Figure 3: A center-cracked panel of infinite plate loaded at the remote boundaries.

both quantities are considered to be the main measures of toughness. The simple expre-ssion for K_c, at the tip of length 2a, in the centre of an infinitely wide sheet subjected to a tensile stress acting in the direction perpendicular to the axis of the crack, is placed by:

$$K_c = \sigma Y \sqrt{a} \tag{5}$$

Y - the geometry correlation factor.

For different testing method and specimen, eq.5 can be modified according to the geometry correlation factor. The fracture toughness and geometry correlation can be expressedin the following formulas (Turner, 1983):

$$K_c = \frac{F_{max}}{BW} Y\left(\frac{a}{W}\right) \bullet \sqrt{a} \tag{6}$$

and

$$Y\left(\frac{a}{W}\right) = 29.6 - 185.5\left(\frac{a}{W}\right) + 655.7\left(\frac{a}{W}\right)^2 - 1017\left(\frac{a}{W}\right)^3 + 638.9\left(\frac{a}{W}\right)^4 \tag{7}$$

where:

F_{max} - the maximum tensile load

B - the thickness of specimen

W -the specimen width

$\left(\frac{a}{W}\right)$ should satisfy $\frac{a}{W} \le 0.5$

Thermoplastics and some of the short fibre reinforced thermoplastics are not brittle at room temperature, and they exhibit extensive plastic deformation. Moreover, these materials are not crack sensitivity at room temperature. Fraster and Ward (Fraster and Ward, 1977) applied a fracture mechanics analysis to results obtained on specimens of polycarbonate bearing notches with various tip radii and concluded that only in the case of razor-notched specimens is it possible, with complete certainly, to interpret the data directly in terms of fracture toughness. Specimens with blunter notches give self-consistent results and higher values of fracture toughness.

2.3. Experimental Procedures

2.3.1. Determination of fiber length distribution and arrangement

Chopped glass fiber reinforced PP with 5,10, 20 and 30% percent fiber by weight (w/o) and neat PP plaques, produced by injection molding were received from Himont Inc, Lansing, Michigan. The dimensions of the molded plaques were 101.6 mm $\times$ 25.4 mm $\times$ 3.2 mm. Fibre length or aspect ratio and the arrangement of fibers in the short fiber reinforced composites are very important parameters to affect the mechanical properties of the material. It was necessary to frist determine the fibre length and fiber arrangement in the thickness before analysis of the GF-PP fracture properties could be perfomed.

The process was begun by cutting a small piece of each composite and putting them in separate clean aluminum pans, then heating them in an open oven at about 400 ^{o}C until the resin was burned off completely. The next step invoved gently placing the fiber remaining from each of the corresponding composites into water gently then depositing them onto filter papers.The fibre length, up to a total number of 200, were then measured under a microscope. The fiber length distribution and the average length for each composite was determined.

Injection molding of short glass fiber reinforced PP often resultes in a natural laminate or layer structure across the thickness. To observe the fiber arrangement across the thickness, (the shaded plane), a small piece of each specimen at the center of the strip was cut from each composite as shown in Figure 4. These samples were polished to diffent

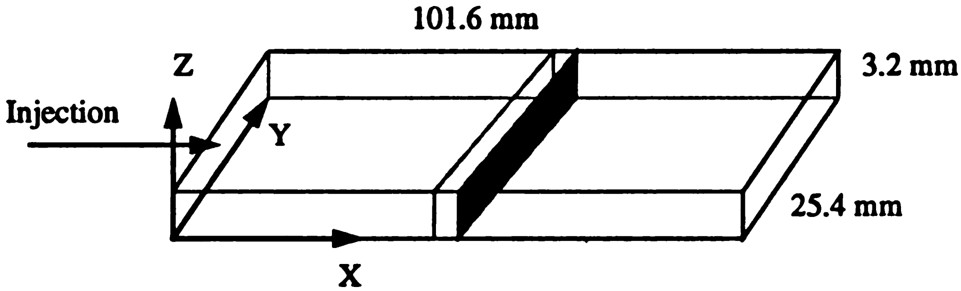

Figure 4: Technique for cutting samples to detect fiber orientation in injection molded short GF-PP plaque

depth and observed under an optical microscope.

2.3.2. Fracture Toughness Testing

The values of fracture toughness of short glass fiber reinforced PP were determined using the sharp notched compact tension configuration according to ASTM (D5045-1992). Location of CT specimen with respect to injection direction and its dimensions are shown in Figure 5. (a) and (b). The sharp notch was created by tapping the sample with a liquid nitrogen cooled blade. Two types of precrack, longitudinal (L-notch) and transverse (T-notch) to the injection direction, were made in the CT specimen in order to taking into account the effect of the fiber arrangement in the thickness direction on the fracture toughness. The fracture tests were conducted on a XI-6 series Instron mechanical testing machine under displacement control. All compact tension tests were performed at a constant crosshead speed of 2.54 mm/min, and at a temperature of about -87^{o}C achieved by imbedding the CT specimen into dry ice in a chamber. The temperature was recorded by a thermocouple and the fluctuation of the temperature during the test was within ±5^{o}C.

The fracture toughness in terms of the critical value of the stress field intensity factor, K_c, was calculated using equation 6. Each result represents the average of five tests. After testing, the fracture surfaces of the specimens were coated with gold by vacuum evaporation and examined by a Scanning Electron Microscope (SEM).

2.4. Experimental Results and Discussion

2.4.1 Fiber Length Distribution in GF-PP

Figure 6 shows the distribution of fibre length for the short glass fiber reinforced PP with various fiber content. The average fiber lengths, $\bar{l}$, in 5%, 10%, 20% and 30% (w/o) are about 0.85 mm, 0.80 mm, 0.70 mm and 0.64 mm respectively. The diameter of the glass fiber is about 14 μm. The fiber length decreases slightly with increasing fiber volume fraction, which causes fiber-fiber interaction during the mixing of fiber and matrix

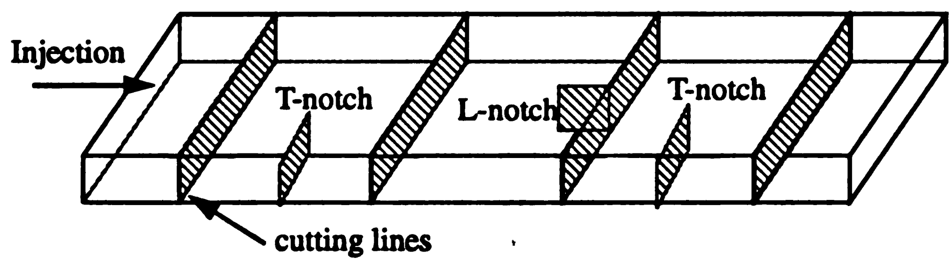

(a)

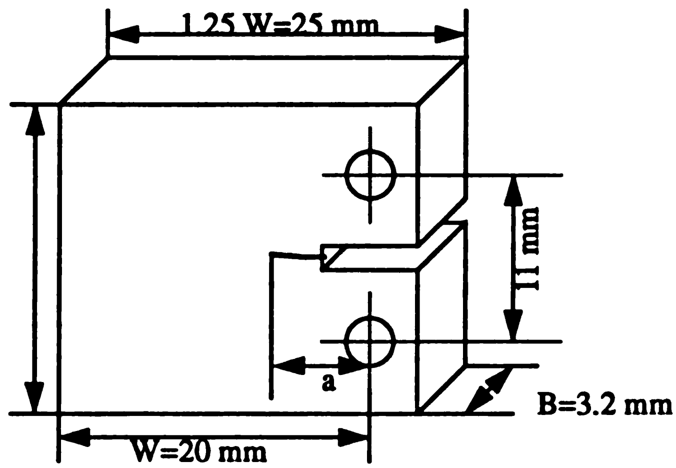

(b)

Figure5: (a) shows how to cut CT specimens from the received injection molded PP and GF-PP plaque and (b) the geometry and dimensions of CT-specimen according to ASTM.

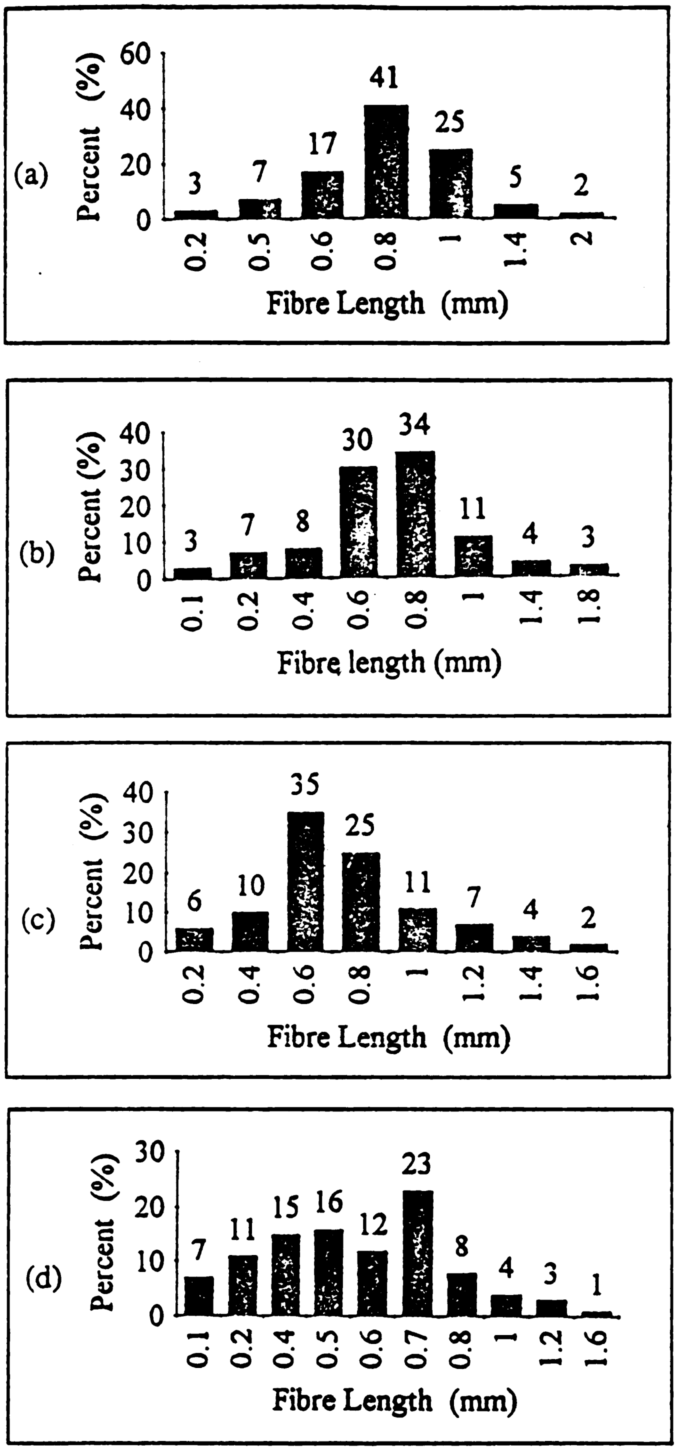

Figure 6: Illustrates the distribution of fibre length (mm) in the injection molded short GF-PP by number percent: (a) for 5% (w/o); (b) for 10% (w/o); (c) for 20% (w/o) and (d) for 30% (w/o) GF-PP.

and the injection molding process. The difference in the fiber length in GF-PP with various fiber content is not a factor affecting the fracture toughness. This can be concluded from the result achieving the maximum toughening by rod-shaped particle when the aspect ratio is above 12 (Faber and Evans, 1983). The aspect ratios of most the fibers are above this value, which can be determined from the distribution of the fibers in Figure 6.

2.4.2. Fibre arrangement across the thickness of the molded plaques

Figure 7 (a), (b), (c) and (d) show microscopically the arrangement of the fibers across thickness (YZ plane) of injection molded short glass fiber reinforced PP with 5%, 10%, 20% and 30%(w/o) respectively. The small circles represent those fibers arranged along the injection direction (X-axis), and the ellipsoids represent those fibers misoriented along X-axis. It could be found that those fibers in the center region, (C), occupy about 0.90 mm, which is one quarter to one third of thickness of a molded plaque. At both side regions, (S), most fibers are arranged randomly. This sandwich-laminate structure in the thickness is obvious, especially in the plaques with fibre content higher than 10% (w/o). Thus, the injection molded short glass fiber reinforced PP can be featured as a layer-structure in which there is a center region, (C), where most fibers are arranged along the injection direction, and in which at both side region, (S), the fibres are random in the thickness direction. This layer-structure is symmetric about the center as shown in Fig. 8, schematically.

2.4.3. Toughening Mechanisms in Short GF-PP

Notched compact tension specimens of PP and short GF-PP were tested by static tension load at dry ice temperature (-87 ^{o}C). The typical deformation of load-opening displacement are illustrated in Figure 9, with curves-1, 2 representing PP and 30% (w/o) with T-notch respectively. The deformation curves of 5%, 10% and 20% (w/o) are between the curves of PP and 30% (w/o). From the deformation curves, the fracture

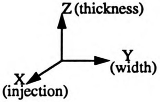

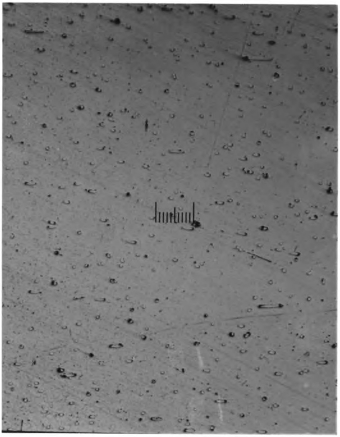

(a)

Figure 7: (a) Fiber arrangement in YZ plane of 5% (w/o) GF-PP (X50)

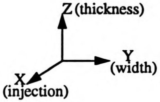

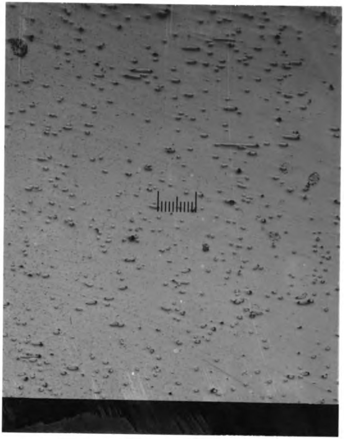

(b)

Figure 7: (b) Fiber arrangement in YZ plane of 10% (w/o) GF-PP (X50)

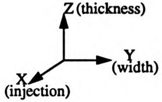

(c)

Figure 7: (c) Fiber arrangement in YZ plane of 20% (w/o) GF-PP (X50)

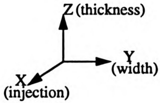

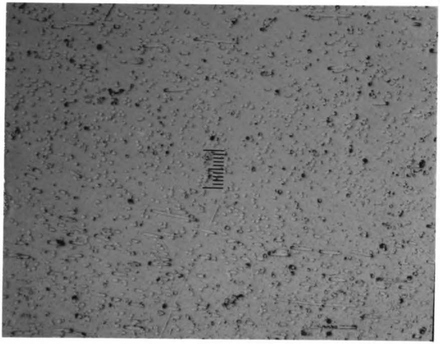

(d)

Figure 7: (d) Fiber arrangement in YZ plane of 30% (w/o) GF-PP (X50)

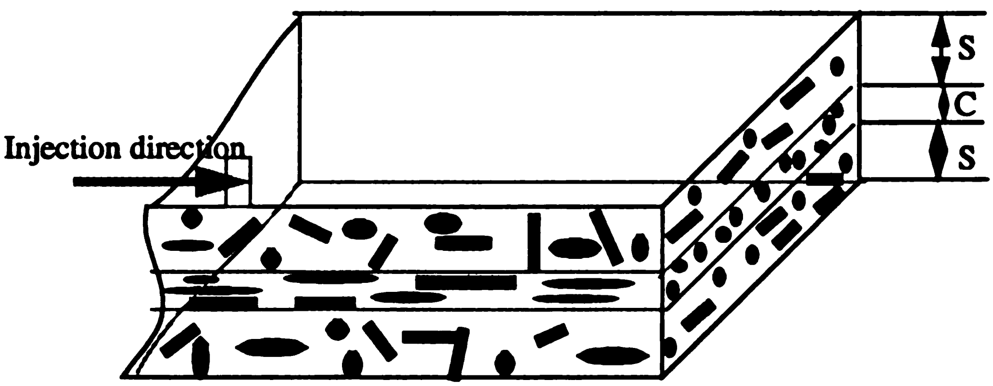

Figure 8: Injection molded induced layer structure in short GF-PP plaque. S indicates side region and C-center region, schematically.

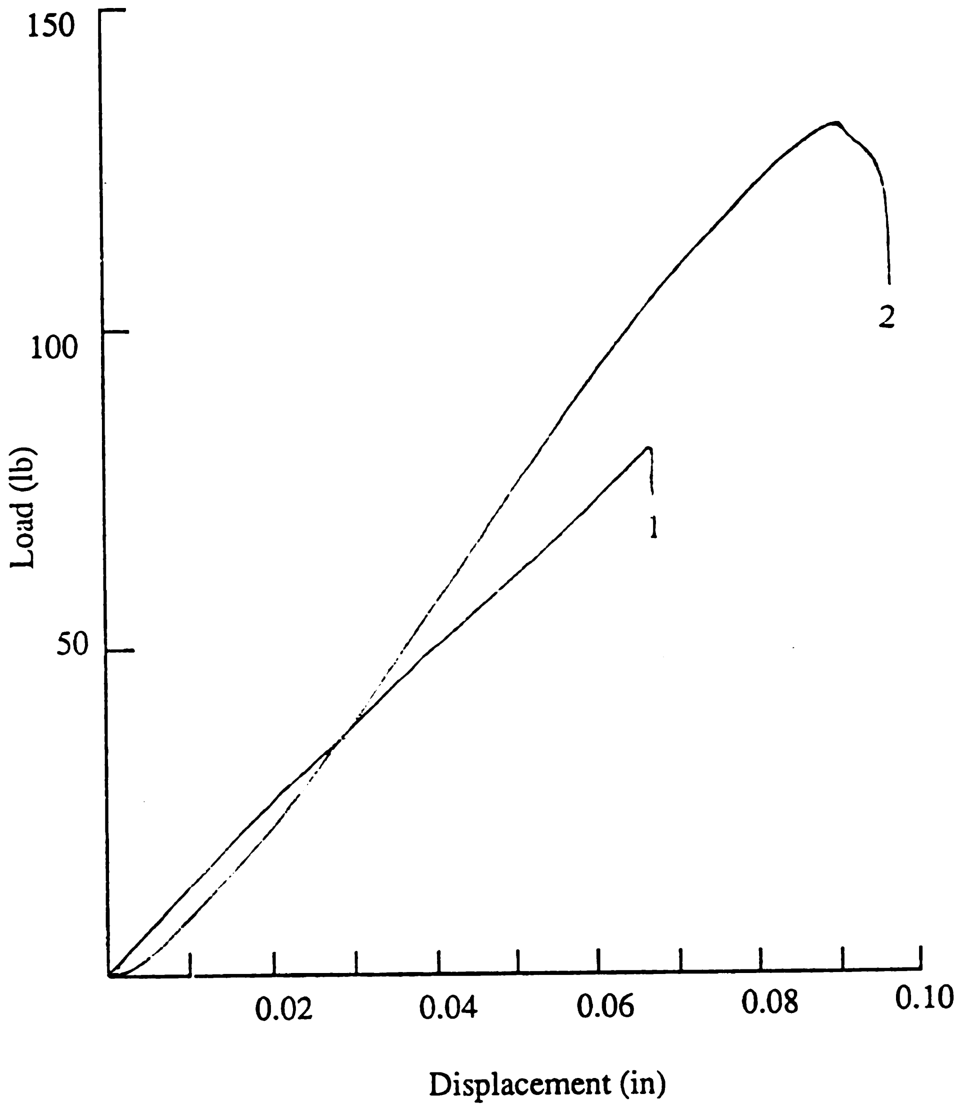

Figure 9: The deformation of notched CT specimens of PP and GF-PP under static load by load-opening displacement, 1 for PP, 2 for 30% (w/o) GF-PP with T-notch.

behavior of notched CT specimens of PP and GF-PP can be recognized approximately as a linear brittle fracture.

Table 1 lists the fracture toughness in terms of the critical stress intensity factor, K_c, and data of neat PP to 30% w/o GF-PP with L-notch and T-notch.

Table1. Fracture Toughness, Kc, of PP and GF-PP

specimen	K_c $(MPa \bullet m^{1/2})$	standard deviation
Neat PP	4.23	0.15
5% w/o L-notch	4.97	0.22
5% w/o T-notch	5.30	0.14
10% w/o L-notch	5.81	0.17
10% w/o T-notch	5.93	0.25
20% w/o L-notch	5.97	0.29
20% w/o T-notch	6.36	0.20
30% w/o L-notch	6.26	0.29
30% w/o T-notch	6.63	0.22

Figure 10 is the plot of fracture toughness with the fiber content for L-notch and T-notch.This illustrates that the value of K_c increases fast from PP to 10% (w/o), then goes up slowly from 10% to 30% (w/o), both for L-notch and T-notch CT specimens. The incremental differences in the fracture toughness of GF-PP, in accordance with to the fiber content, indicate that the toughening mechanisms might be varied with the fiber contents.

The toughening mechanisms of GF-PP and the mechanism of energy-absorping in pure PP are discussed as follows:

2.4.3.1. Mechanism of Energy-absorption in PP

The value of fracture toughness of notched CT specimen of PP is 4.23 $MPa \bullet m^{1/2}$

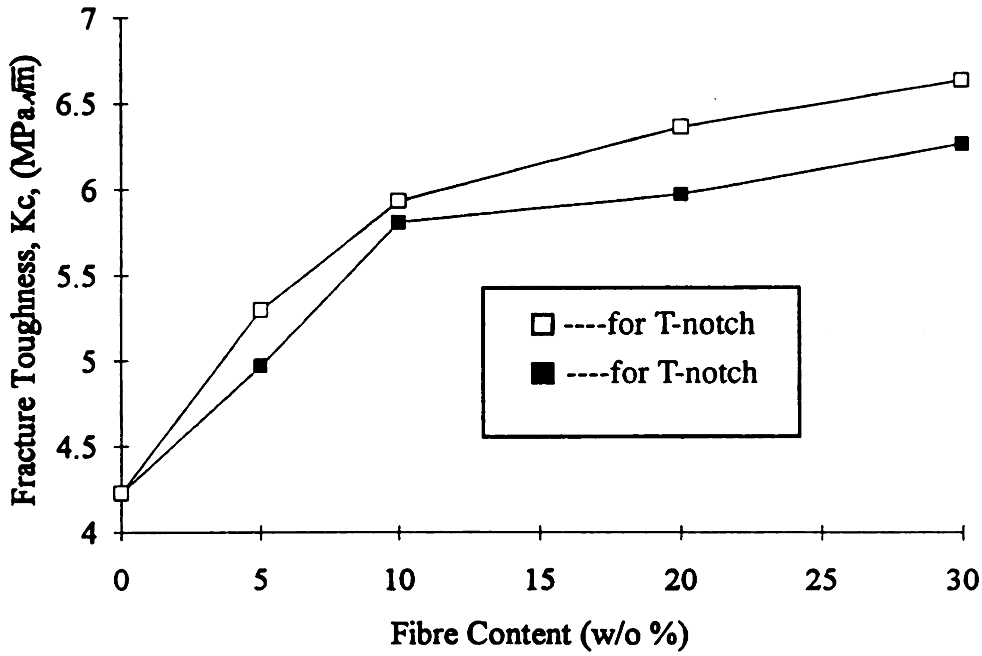

Figure 10: Fracture toughness, Kc, of notched CT specimens of PP and short GF-PP under static load and at low temperature (-87 ^{o}C).

at the testing conditions. This value is quite high compared with other polymeric materials (Kausch, 1978). This indicates that the matrix itself has good crack resistance at low temperature.

Figure 11 is a SEM micrograph representation the fracture surface of PP near the notch root, which shows a dimple pattern of deformed matrix in this region. It must be accepted that the dimple pattern of deformed polymer matrix is characteristic of crazing in the amorphous and semi-cystalline polymers (Friedrich, 1983). In the study of polymer fracture, it has been concluded that crazing plays an important role in the failure of PP at a range of temperature from -200 ^{o}C to 150 ^{o}C (Kitagawa et al. 1984). The formation of the dimple pattern in this fracture surface can be explained from the spherulite structure of semi-crystalline PP. The spherulites are pointed, nucleated semi-crystalline entities which grow in a spherically symmetrical form until their boundaries impinge. The fibrils formed from the amorphous part near the boundaries of the spherulites under normal load. Inside the spherulite, is a crystal structure, therefore, the plastic deformation is confined to the weak spherulites boundaries and results in a typical dimple fracture pattern. The failure of fribril, either by continued chain reparation including slippage and disentanglement of molecular coils, or through scission of entangled chains (Hannon, 1974). Friedrich (Friedrich, 1983) concluded that under plane strain condition (favored by sharp notch, low temperature), crazing provided a mechanism for absorption and dissipation of fracture energy.This explains pure PP could retain a relatively high fracture toughness, even at a temperature below its glass transition temperature.

2.4.3.2 Low fibre content of GF-PP

Figure 10. shows that the fracture toughness increases quickly from 5% to 10% (w/o) and the relationship of Kc to the fiber content is approximately linear (for example, the plot of T-notch specimens). This phenomenon can be explained as a crack pinning mechanism, in which the rigid short glass fibers act as obstacles and force the cracks to

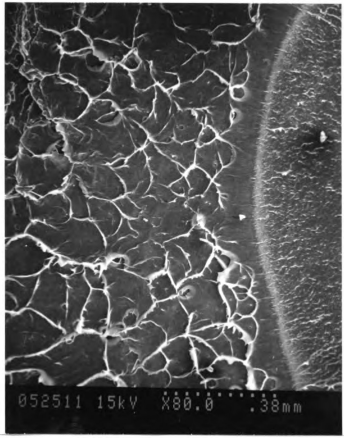

Figure 11: SEM micrograph of fracture surface of notched CT specimen of PP near the notch root showing dimple pattern of the deformed matrix.

bow between them. Figure 12 and Figure 13. represent the fracture surfaces near the notches of 5% and 10% (w/o) GF-PP with T-notch respectively. The existence of "tails" behind the fibers on the fracture surface has been cited as evidence of crack pinning mechanism in particle reinforced resins (Kinloch and Young, 1983). Those "tails" were formed behind the fibers (pull-out fibers or broken fibers) as a result of the interaction between the propagating cracks and the fibers after the crack front had broken away from the latter. The fracture surfaces appear flat except for the localized matrix deformation around the fibers and homogeneous deformation in the large fiber avoid areas.

From the above observations, it is believed that crack pinning can be used to explain the toughening mechanism of short glass fiber reinforced PP at low temperature. The increase of fracture energy is proportional to the inverse of the interparticle spacing (D). The best approximation for the interparticle spacing between randomly arranged rod-shaped particles (short fibres) is that given by Bansal and Ardell (Bansal and Ardell, 1972), where the center-to-center nearest neighbor spacing between finite parallel cylinders

$$\frac{D}{d} \approx \frac{e^{4V_f}}{V_f^{\frac{1}{2}}} \int_{4V_f}^{\infty} x^{\frac{1}{2}} e^{-x} dx \tag{7}$$

where V_f is the volume fraction of fiber, and d is the diameter of fiber. D can be determined in the GF-PP as about 95 μm, 54μm,39μm, and 28μm for 5%w/o(2% vol), 10% w/o(4% vol), 20% w/o(8% vol) and 30% w/o(13% vol) respectively. According to the results in studies of short carbon fiber reinforced polyphenylene sulphide (PPS) and phenolphthalein side-group polyethersulphone (PES-C) thermoplastics by Lin and Lai (Lin and Lai, 1993), and the reports in other cracking pinning systems (Lang and Radford, 1971), it was found that the fracture energy increased linearly with D varying from infinite to about 40μm. Smaller D revealed little effect on the increment of the fracture energy. However when the spacing is larger than 40μm, the crack is "flexible" allowing the crack

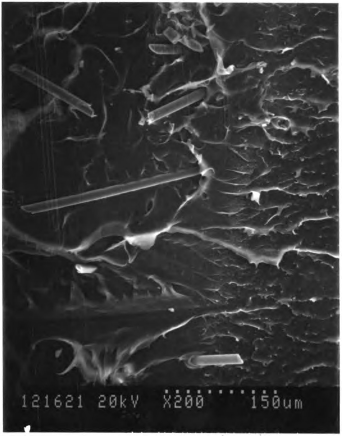

Figure 12: SEM micrograph of fracture surface of notched CT specimen of 5% (w/o) GF-PP with T-notch near the notch root.

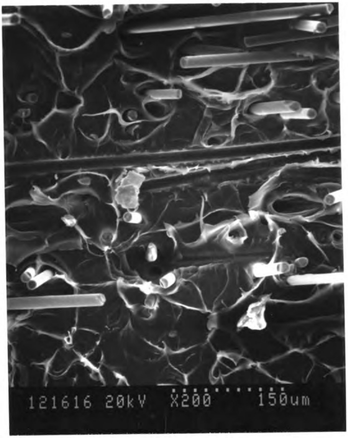

Figure 13: SEM micrograph of fracture surface of notched CT specimen of 10% (w/o) GF-PP with T-notch near the notch root.

front to bow out between the particles, thereby forming secondary cracks under the action of the driving force. Thus, energy is required not only to create the new fracture surface but is also supplied to the newly formed non-linear crack front, resulting in an increase of fracture energy or fracture toughness. When the value of D decreases further, the flexibility of the crack reduces and the crack pinning mechanism is no longer valid for predicting the fracture toughness any longer. Thus, the crack pinning in GF-PP with fiber content below 10% (w/o) fractured at low temperature is the main toughening mechanism.

2.4.3.3 High Fibre Content of GF-PP

The crack pinning and crack deflection processes usually occur simultaneously. Crack pinning produces a non-linear crack, and crack deflection produces a non-planar crack. Figure 14 and Figure 15 represent the fracture surfaces near the notch roots of 20% (w/o) and 30% (w/o) with T-notch respectively, which display non-planar fracture surfaces. Although post-failure examination of fracture surfaces does not allow determination of the precise path and direction of the crack (or a trace of the crack front) at any instant during propagation, it is capable of providing valuable information about the crack deflection profile (Faber and Evans, 1983). Thus, the existence of crack deflection in the fracture process of 20% and 30% (w/o) GF-PP is possible and reasonable.

The plot of the mathematical model, based on a fracture mechanics approach, is shown in Figure 16 for three aspect ratios (Fraber and Evans, 1983). It predicts that the toughening increment becomes a volume fraction invariant above ~0.2. The influence of the aspect ratio tends to be an asymptotic limit at larger values of 12. The fracture toughness of notched CT specimens of GF-PP slowly increment from 10% w/o (4% vol) to 30% w/o (13% vol) in this expriment is consistent with the result predicted from Figure 16, which shows in the range of fiber volume fraction from about 0.05 to 0.2.. Greater amount of fibre content may diminish the toughness increase due to overlapping particles. The phenomenon of overlapping fibres in the fracture surfaces are shown clearly in Figure 14

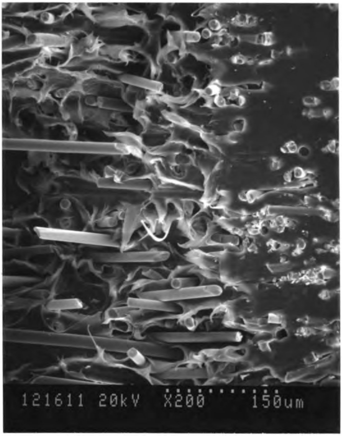

Figure 14: SEM micrograph of fracture surface of notched CT specimen of 20% (w/o) GF-PP with T-notch near the notch root.

Figure 15: SEM micrograph of fracture surface of notched CT specimen of 30% (w/o) GF-PP with T-notch near the notch root.

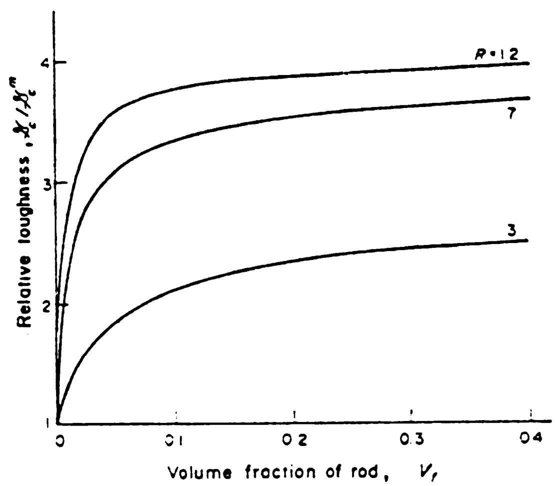

Figure 16: Relative toughness predictions from crack deflection model for rod-shaped particles of three aspect ratios (Faber and Evans, 1983).

and Figure 15.

In addition to the crack pinning and crack deflection mechanisms of toughening, fiber pull-out, homogeneous and localized plastic deformation of the matrix, debonding of the fiber-matrix interfaces and a few fibers broken, are also very important absorbing energy mechanisms in the fracture of short glass fiber reinforced PP. The evidence for all of these fiber-related failures can be observed from the fracture surfaces both in the low fiber and high fiber content specimens (Figure 12 to 15.)

2.4.4 The Effect of Fiber Arrangement on The Fracture Toughness

For the same fiber content of CT specimen, a T-notch has a higher value of fracture toughness than that of a L-notch specimen. This can be explained through the layer structure in the thickness of injection molded short glass fiber reinforced PP plaques. The fiber arrangement in the T-notch and L-notch can be illustrated schematically as Figure 17 (a) and (b), respectively. In the notched plane of a CT specimen with a T-notch, there is a center region, (C), in which about one-fourth to one-third of those fibers are arranged transverse to the notch direction, and the fibers are random in the both side regions, (S). On the other hand, in a L-notch specimen, those fibers in the center region are longitudially arranged along the notch direction, and fibers are random at both sides. In this case, there are a relatively larger number of fibers which are arranged nearly perpendicular to the advancing crack front in the T-notch samples. The transversely arranged fibers can contribute much more effectively to the strength of the material in front of the starter crack, and require higher loads to force those cracks to move forward. If, on the other hand, more fibers are located in plane , almost parallel to the crack direction, the crack could propagate along the fiber sides by void formation and cause fibre/matrix debonding which has less effective crack hindrance effect (Friedrich, 1989). Figure 18 represents the characteristic fracture surface of 20% (w/o) GF-PP with a L-notch showing the area in the center region, (C). Comparing Figure 18 to Figure 14 (20% w/o with T-notch and taken from the center region of the thickness) it can be observed clearly, that more fibers are arranged longitudially to the notch root in 20% (w/o) CT specimen with L-notch, however more fibers are arranged transverse to the notch direction in the latter. This explains the reason why the value of fracture toughness of the specimen with T-notch is higher than that of the with L-notch.

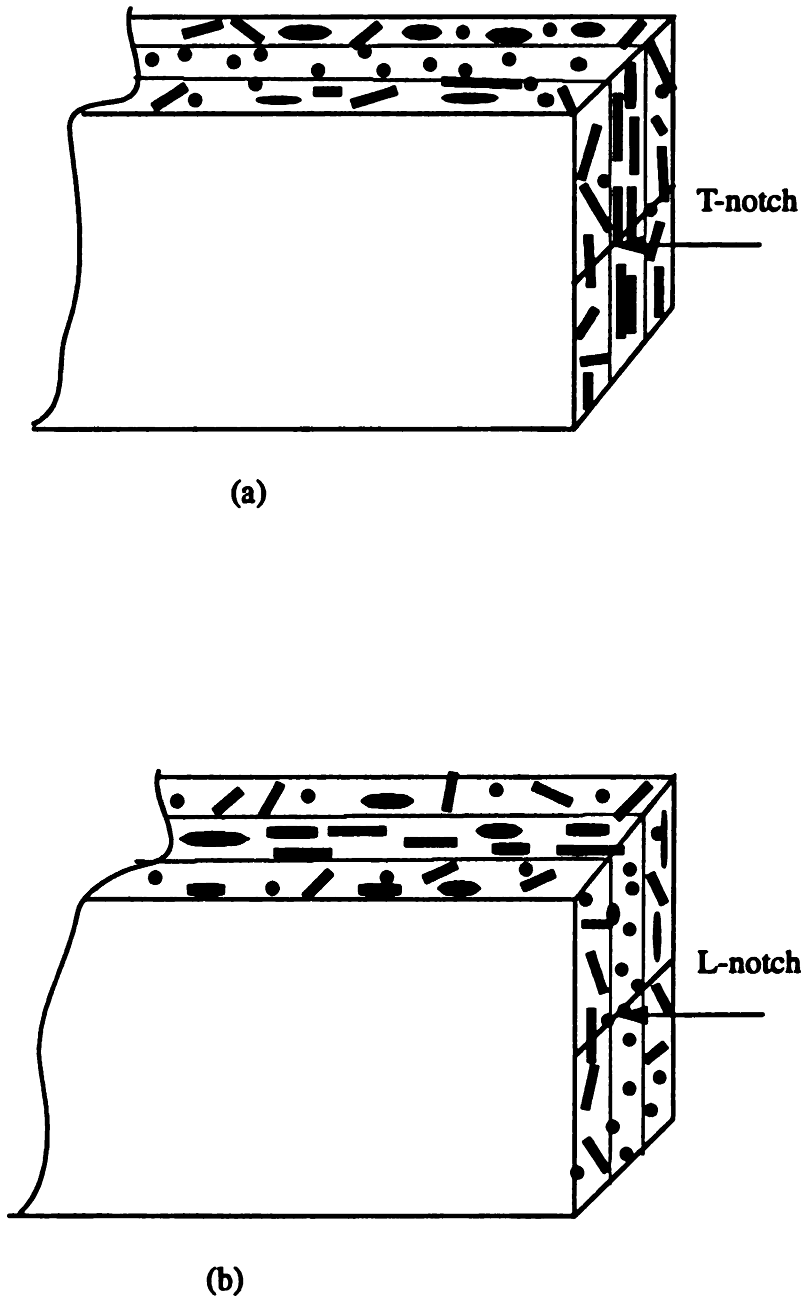

Figure 17: Schematics to show fibre arrangement in T-notch (a) and L-notch (b).

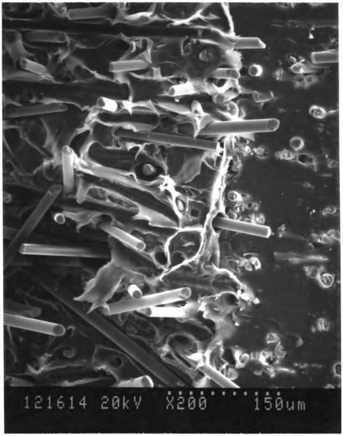

Figure 18: Characteristic fracture surface of 20% (w/o) GF-PP with L-notch shows large number of fibres were arranged parallel to the notch.

2.5 Summary

The increment of fracture toughness, is dependent on the fiber content at low temperature. When fiber content is low (from 5% to 10% w/o), Kc increases rapidly and the mechanism of toughening can be explained by crack pinning. However, the fracture toughness increases at a slower rate when fiber content is above 10% (w/o), and the toughening mechanism explained by crack deflection. In addition, other energy consuming mechanisms intervene during crack propagation and exist simultaneously, such as fiber pull-out, plastic deformation of matrix (homogeneously and localized), debonding of the fiber-matrix interfaces and a few fibers broken. Under current testing conditions, crazing provided a mechanism for absorption and dissipation of fracture energy for notched specimen of PP.

It was found that the CT specimen with T-notch has a higher value of fracture toughness than that with L-notch for the same fiber content. This is because more fibers were arranged transverse to the prenotch in the T-notch specimen than that in the L-notch specimen according to the layer structure of injection molded GF-PP.

CHAPTER 3

Welding of PP and Short Glass Fiber Reinforced PP

3.1 Introduction

Welding or healing of amorphous polymers was studied widely both experimentally (Jud et al., 1981 and Wool et al. 1982) and theoretically (de Gennes, 1980, Kim and Wool, 1981, Prager et al. 1980) based on the reptation theory which was developed by de Gennes (de Gennes, 1971). De Gennes considered the movement of a single chain in a fixed network, which although an ideal case, gives very good results conformed by experiments for amorphous thermoplastics.

The reptation theory predicts that the length of the chain ends (or called minor chains) varies with the square root time. Later, wool and Kim combined the reptation theory of self-diffusion in polymer melt with molecular criteria, which include molecular weight, the number of chains, number of bridges, average monomer interpenetration depth, etc., describing the relationship of healing processing time and the macroscopic mechanical properties, such as interfacial strength and fracture toughness. Their theoretical model states that the energy of fracture is proportional to the number of chain segments spanning the interface, and obtained the fracture stress is proportional to the fourth root of time. Those results are in agreement with the experiments of healing amorphous polymers conducted by Jud etc., (Jud et al., 1981, and Wool and O'Connor, 1982).

The study of welding thermoplastic composites was carried out by Bastein and Gillespie (Bastein and Gillespie, 1991). They used the reptation model to predict the fracture stress and energy as a function of the process history including temperature and time. However, their model is restricted only to the amorphous thermoplastic composites, because they used an amorphous film bonding technique, by which placed a thin film of amorphous material in the interface.

Although there have been some investigations into the welding of semi-crystalline polymers and their composites by Stokes (Stokes, 1988, 1991) and Andrew and Bevis (Andrew and Bevis, 1984), they concentrated in the fields of developing welding methods and the effect of processing parameters on the strength of butt joints. In these experimental studies, the welding temperature were chosen above the melting temperatures of the matrix and thus, the welding processes depended upon the molten flow. The interface between the two parts disappeared at the instance of keeping the two parts intimate contact. There is not a successful model to predict the interfacial strength and fracture energy for welding semi-crystalline polymers and their composites. The investigation of the relationship of the interfacial strength of semi-crystalline polymers and their composite joints is very important.

In this study, the effect of the processing time and temperature on the interfacial strength development of welding PP to short glass fiber reinforced PP and GF-PP to itself was carried out. The fibers in the weld region involved in the failure of the welded specimen was taken into consideration.

3.2 Background

3.2.1 Strengthening Mechanisms of Short Fibre Reinforced Thermoplastics

In the case of continuous fibre reinforcement, all the fibers were working at maximum efficiency, with the average strain in the fiber being equal to that in the matrix. Assuming that bonding of the interface between fiber and matrix is perfect, the tensile modulus in the tensile direction; modulus of the composite can be estimated as equation 8,

$$E_c = E_m \phi_m + E_f \phi_f \tag{8}$$

and the modulus, E_{ct}, in the transverse direction can be estimated by equation 9.

$$\frac{1}{E_{ct}} = \frac{\phi_m}{E_m} + \frac{\phi_f}{E_f} \tag{9}$$

where E_c,E_m and E_f are tensile moduli of the composite, matrix and fiber respectively. ϕ_m and ϕ_f are the volume fractions of the matrix and the fibers in the composites.

It is more difficult to deal with the short fiber reinforced composites due to the complication of a spectrum of fibre length and orientations caused by manufacturing processes, such as injection molding and extrusion. An earlier study on the strength of short fiber reinforced thermoplastics was carried out by Cox (Cox, 1952). The calculation of the variations in the shear and tensile stress along a short elastic fibre in a plastic matrix, was estimated by elastic mechanics. In aligned short fibre composite, Figure 19, shows the state of deformation around a short fibre. The fibre restricts the deformation of the surrounding matrix, because it is stiffer than the matrix material. The load is transferred from the matrix to the fiber throught the interfacial shear stresses. The shear stress is greatest at the end of the fiber, and decays to zero some where along it's length. The tensile stress is zero at each end of the fiber and reaches a maximum at the center. If the fiber is at a length equal or greater than the critical elastic aspectic ratio, $(\frac{L}{D})_c$, the maximum tensile stress reaches the tensile stress of the fiber. Figure 20. summarizes the results.

3.2.2 Fracture mechanisms of Semi-crystalline polymer

The problem of deformation behavior of semi-crystalline polymers becomes more complicated when a crystalline-amorphous microstructure of the polymer must be considered. Brady and Yhe (Brady and Yhe, 1981) showed that the crystalline spherulites deformed only after substantial deformation had already occurred in the interconnecting amorphous regions. Crazing and shear-banding were the primary modes of the deforma-

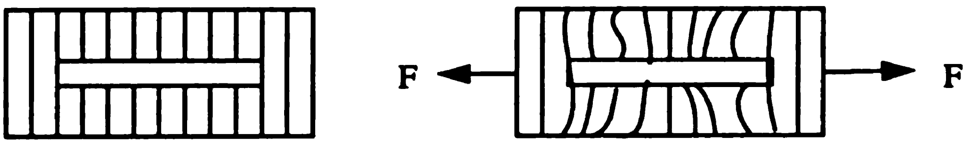

(a) Before applying load (b) Under tensile load

Figure 19: The effect of a fibre on the matrix deformation.

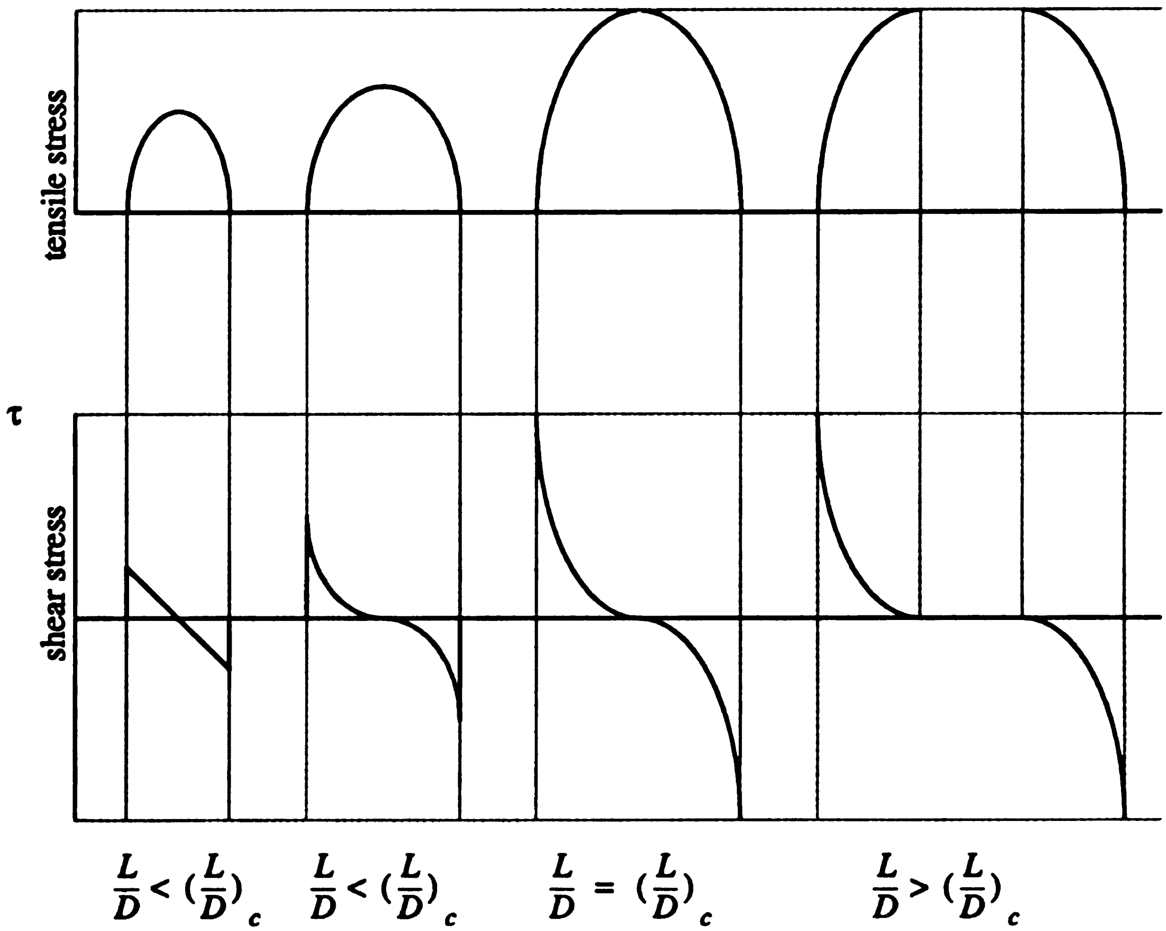

Figure 20: The tensile stress and shear stress distribution along a fibre.

tion mechanisms for semi-crystalline polymers.

The formation of crazes in semi-cystalline thermoplastics is a common response to an applied tensile stress. Under plane strain conditions, (favored by thick sections, sharp notches or at low temperatures), crazing provides a mechanism for absorption and dissipation of energy. In the past, craze-like features have been frequently observed during the studies of semi-crystalline polymers, although they were sometimes named differently, such as "strain bands" in fibres of PA, PETP, PE and PP, "cracks" and "microcrack" in PP and PA 6, in certain literatures (Olf and Peterlin, 1974). The craze formation in bulk semi-crystalline thermoplastics has been concluded by Friedrich (Friedrich, 1983) as the following three steps:

I. First of all, at sites of enhanced stress concentration, (i.e at preexisting voids in the microstructure or at sites where amorphous layers between lamellae are oriented nearly under 45° to the applied load), a local sliding occurs between individual lamellar ribbons having only a low degree of entanglment in their common amorphous interlayer. At this stage, strain is accommodated almost entirely by the interlamellar amorphous regions. During this process the crystals change their orientation, and the shear stress component decreases, while the stress in direction of the molecular axis of the crystals increases.

II. In a secondary step, once the local tensile stress reaches a critical value (equal to the stress at which macroscopic yielding can take place), individual blocks are pulled out of the crystal ribbons. Due to this local yielding process, submicroscopic defects, having an ellipsoidal shape, are created between the lamellae. However, the defects are able to cause an increase in stress in their lateral neighborhood, consequently involving adjacent lamellar ribbons in the local deformation process. Thus, the probability for further creation of voids, as well as for formation of fibrils between these voids, is increased.

III. The third step is the longitudinal transmission of strain onto connected crystalline blocks and leads to a perfect stretching of these fibrils. As the fibrils are able to stabilize the enhanced microvoid volume between them, a lateral coalescence of these voids finally provides a local deformation zone in the shape of a craze, as known from amorphous polymers.

Figure 21. is a schematic diagram for these three steps.

The formation of shear bands of semi-crystalline polymers during deformation has been found only when it was loaded by compression and at the temperature lower than 0.75 T_g (Friedrich, 1983). Few comprehensive studies exist which consider the formation of shear bands for semi-crystalline polymers.

3.2.3 Fracture Mechanisms of Short Fiber Reinforced Thermoplastics

Short fiber in thermoplastics can transfer the load from matrix to fiber and result in greater strength, as well as other mechanical properties. The mechanisms of the fracture of the composite are complicated because they are greater affected by the fiber length, the fiber orientation and the fiber/matrix bond strength.

It seems that Sato et al. (Sato et al., 1984) studied the mechanism of fracture of short fiber reinforced thermoplastics comprehensively. In their study, short glass fibrer reinforced polyamide 6.6 was investigated by in situ SEM. It was found that there were three stages within the failure. Under a tensile load, the stress concentration occurs in the vicinity of fibers, especially at the fiber ends. Under the influence of the concentration stress, cracks may occur at the fiber ends. This is the first stage of failure. While the shear deformation of the matrix along the fiber sides increases with stress, the interfacial cracks propagate from the fiber ends along the fiber sides due to the shear deformation of the matrix in the second stage of the failure. With the occurrence of the these cracks, the load bearing capability of the fibers is greatly reduced, and the matrix is required to support a greater load. The matrix cracks come to grow from the interfacial cracks just prior to the composite failure. These interfacial cracks and matrix cracks may result in a catastrophic

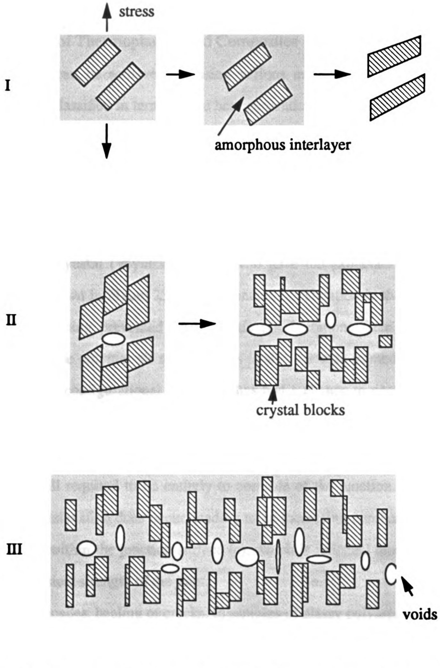

Figure 21: Schematic steps of crazes formation in a semi-cystalline polymer structure

crack propagation leading to the composite failure. This is the final stage of the failure. Even in this stage, fibers are only pulled out from the matrix and without broken. This mechanism of the composite fracture may explain the brittle manner, in contrast to the ductility of the unfilled polymers. The results can be diagrammed in Fig. 22. (a), (b), and (c).

3.2.4. Welding of Thermoplastics and Composites

Welding can be achieved by using various methods for plastics. All of these methods can be classified in terms of the heat generations employed, such as hot gas, hot plate, and infrared welding, etc. In spite of the differences between these welding techniques, the fundamental of all fusion bonding processes is nothing but intermolecular diffusion between surfaces in intimate contact (Bastien and Gillespie,1991).

The earliest systematic study of healing or welding in amorphous polymers was undertaken by Voyuskii (Voyutskii, 1963), who gave the explanation of the molecular interpretion as shown in Figure 23. Before contact, the situation is shown in (a), with the polymer chains being prevented by energetic considerations from extending isolated tendrils through the polymer-air surface. This is also the case immediately after contact, before significant configurational relaxation has had a chance to occur, as shown in (b). Although the density of polymer segments is now the same as in the bulk near the junction surface, the configurational distribution of the polymer molecules certainly is not; since each chain is still required to lie entirely to one side of the junction. In time, of course, configurational relaxation does occur, leading to an increasing number of intersections of polymer chains within the junction surface (c), which is reflected macroscopically in the growing mechanical strength of the joint.

In last decades, healing of cracks, in samples of glassy polymers was studied comprehensively (Jud and Kausch, 1979; Jud et. al, 1981; Wool and O'Connor, 1981). Theoretical models have combined the reptation theory of self diffusion in polymer melts (Gennes, 1971) with molecular criteria describing an increase in interfacial strength

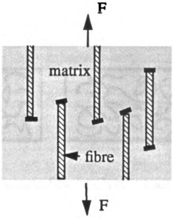

(a) First stage; occurrence of crack at fibre ends

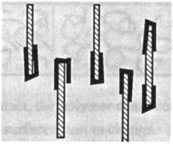

(b) Second stage; propagation of the crack along the fibre sides

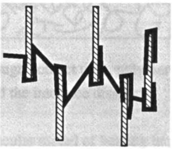

(c) Final stage; occurrence of the crack in the matrix

Figure 22: Model of fracture mechanism of short fiber reinforced thermoplastics.

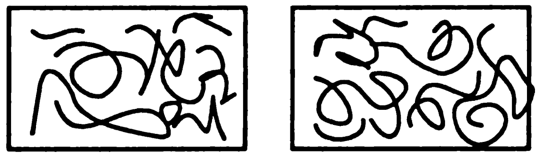

(a) Before contact of two polymer specimen

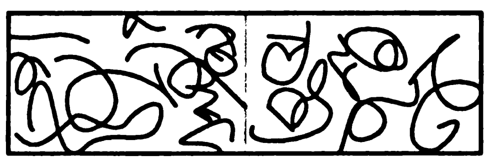

(b) After contact, the polymer chain configurations near two surfaces start to change

(c) After enough contact time, polymer chains relaxiation occur and the interface disappear

Figure 23: Molecular model of healing in polymers.

interdiffusion progresses to predict the time dependence of the healing process.Prager and Tirrell (Prager and Tirrell, 1981) studied the crossing density criterion, which states that the energy of fracture is proportional to the number of chain segments spanning the interface, and obtained an initial $\sqrt{t}$ dependence of the fracture energy in agreement with experimental data. This corresponds to a $\sqrt[4]{t}$ of the growth of fracture stress.

The literature on the welding reinforced thermoplastics is quite small. They are mainly concerned the welding methods (Andrews and Bevis, 1984). Andrews and Bevis investigated the butt-fusion welding of chopped-graphite-fibre-filled polyvinydenefluoride(PVDF) to itself and to the neat material. In their study, it was shown that the weld strength of the filled material was significantly lower than the strength of the filled material. The strength of filled to unfilled material joints could, however, be almost as high as that of the unfilled material. The reduction of the strength in the weld joint of composite to composite was considered owing principally to the off-axis alignment of fibre in the weld plain due to the melt flow in the welding process. Strokes (Stokes, 1991) studied the welding of chopped-glass modified polyphenylene oxide (GF-MPPO) to itself and to the neat material by vibration-welded butt joints with results similar to those involving the joints of PVDF and filled PVDF. Besides off-axis alignment, poor bonding at the fibre-resin interface in the weld zone, is another reason for the strength reduction of the joint.

3.3. Experimental Procedures

3.3.1. Material

The materials which are used to make butt-joints are injection molded PP and 5%, 10%, 20% and 30% w/o GF-PP. In addition to these materials, some ASTM tensile specimens of PP and 5% to 30% w/o GF-PP were also received from Himont company, which can be used as a reference for the study of strength development.

3.3.2 Welding Processing

A welding tool was designed as shown in Fig.ure 25. The heat, generated from the hot plate is transferred through the aluminum tool. The on-axis pressure loading can be applied driving the screw bolt, which moves the aluminum block in the groove. The pressure is controlled by the displacement of scew bolt, in which one turn is equal to $\frac{1}{32}$ inches. This design will provide an even force distribution on the surface of the welding specimen; moreover, it can limit the flow of the melting materials, which produces a weld bead outside the weld region in most other welding methods. In this case, the effect of weld bead on the mechanical properties can be overlooked. The temperature was measured by a thermocouple, and temperature fluctuation was controlled within $\pm 2\ ^{o}C$. The techniques for welding, PP/GF-PP and GF-PP/GF-PP butt-joints are as follows:

(1) The injection molded GF-PP plaque is cut as in Figure 5 (a), to a 26 mm length, with the weld faces perpendicular to the injection direction. The faces to be welded are then polished and parallel.

(2) The whole surfaces of the specimen are cleaned with acetone and dried .

(3) The welding tool is placed in the hot press and the temperature is checked by a thermocouple through a makeup-specimen. When the temperature goes up to the required temperature and equilibriums, two parts of specimen are placed inside the groove and covered . The two parts are then kept in contact by driving the scew bolt, at which point timming of the process begins.

(4) After the faces of the two parts have been held together under a chosen time, temperature, and pressure, the weld tool is taken from the hot press and cooled down by placing it between two large aluminum blocks. At the cooling rate of about 56 ^{o}C/min, it only need 10 seconds are need to cool the specimen from 180 ^{o}C to 165 ^{o}C (at or below this temperature, no joint can be made). The thermal history of the welding process is shown in Figure 26. Due to the short period of time involved with cooling, its effect on the

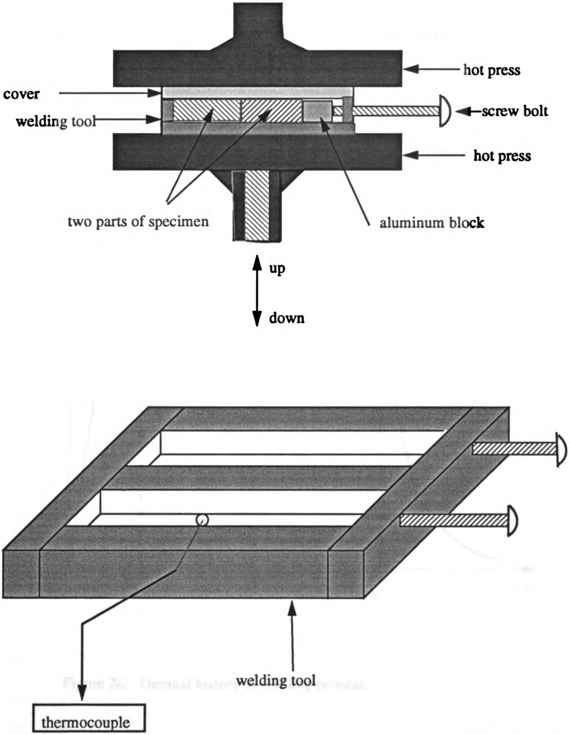

Figure 25: Schematic of the welding tool and equipment.

weld joint is not significant.

(5) When a visually satisfactory weld bar had been produced, the edges and the surfaces, which have thermallyl contracted in the cooling stage, are polished. The dimensions of the final weld bar is 50 mm × 12 mm × 3.0 mm.

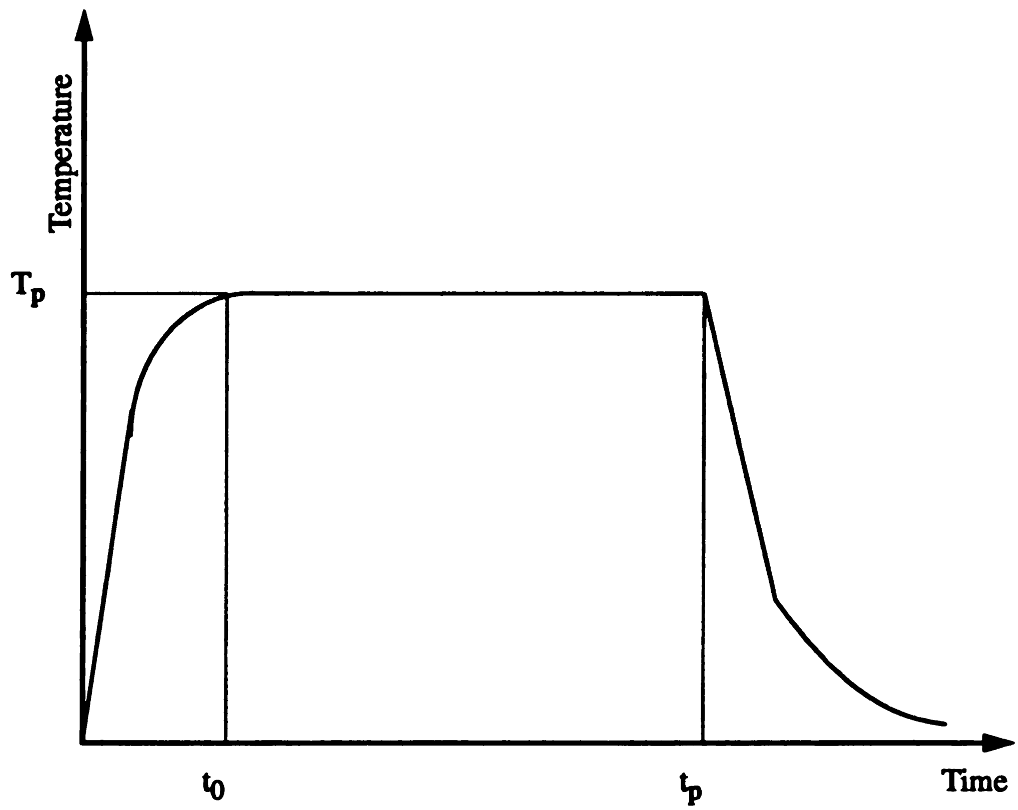

Figure 26: Thermal history of welding process.

3.3.3. Tensile tests

Tensile tests of ASTM tensile specimens and the welded butt-joints of PP/PP, PP/GF-PP, and GF-PP/GF-PP were carried out on a XI-6 series Instron mechanical testing machine at a constant cross head speed of 2.54 mm/min and at room temperature.

3.4. Experimental Results and Discussion

3.4.1. Tensile Properties of Bulk PP and GF-PP

The ASTM (D638-89) tensile specimens of PP and short GF-PP were tapered at the center, with a diameter, d, of 0.08 inches. This was done because preliminary testing of dumb-bell shaped specimen of PP and 5% w/o GF-PP always resulted in failure at one of the grips or shoulders. Therefore, in order to insure that the failure occurs in the range of the gauge region, tapered is necessary, and this method has been used in the tensile test for soft plastics. The tapered hole in the specimen does not effect the peak and yield strength, but eliminates the break strain significantly. Figure 27 represents the load-displacement deformation curves of the injection molded PP and short GF-PP tensile bars, and curves-1, 2, 3, 4, and 5 represent PP, 5%, 10%, 20%, and 20% (w/o) GF-PP specimens respectively.

The results of tapered ASTM tensile specimens are summarized in Table 2.

Table 2:. The results of ASTM tensile specimen

specimen No.	Peak stress (MPa)	Yield stress (MPa)	Young's modulus (GPa)	Break strain (%)
PP	35± 0.3	22.3 ± 1.5	0.80 ± 0.05	13.0 ± 0.8
5% GF-PP	39 ± 1.0	27.0 ± 2.0	0.97 ± 0.03	7.2 ± 0.6
10% GF-PP	44 ± 2.4	33.6 ± 2.5	1.18 ± 0.1	5.6 ± 0.4
20% GF-PP	51 ± 1.6	42.2 ± 3.5	1.52 ± 0.06	4.5 ± 0.3
30% GF-PP	56 ± 1.6	48.2 ± 2.7	1.84 ± 0.06	4.1 ± 0.3

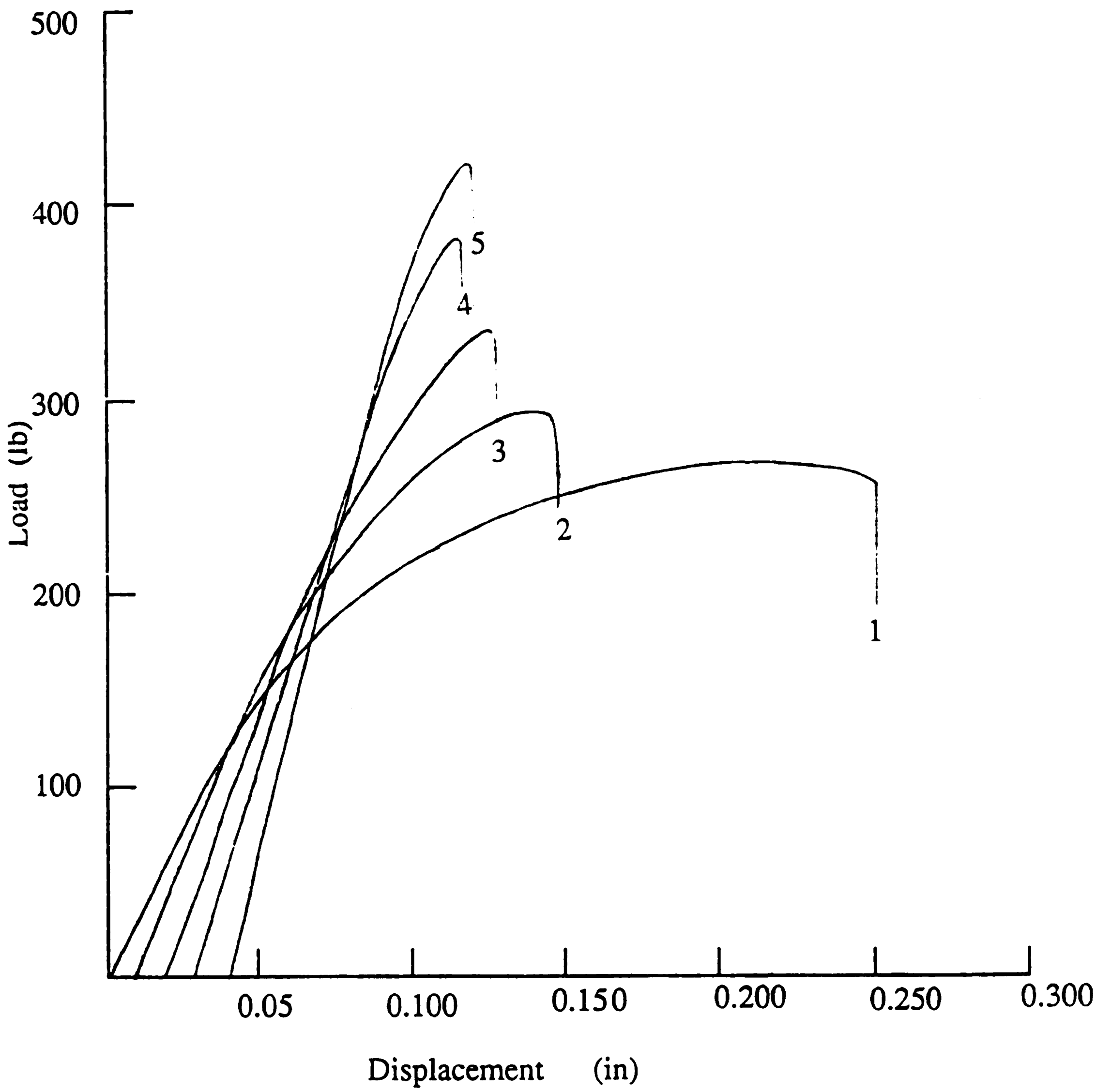

Figure 27: Load-displacement curves for injection molded ASTM tensile bars of PP and short GF-PP with various fibre content (w/o), 1, 2, 3, 4, and 5 present PP, 5%, 10% 20%, an 30% GF-PP, respectively.

In Table 2, it is shown that the peak and yield stresses of composites increase steadily with fibre content. The peak and yield stresses increase about 80% and 100% from PP to 30% w/o GF-PP respectively. Young's modulus increase from 0.8 GPa for PP to 1.84 GPa for 30% w/o GF-PP. However, the break strain decreased abruptly, from PP to 5% w/o GF-PP, and then gradually dropped off with increased fibre content.

Figure 28. represents the typical failure surface of a 30% w/o GF-PP ASTM tensile specimen. From this picture, it can be observed that a large number of holes and outwardly protruding fibres on the failure surface indicates that fibres were pulled out completely during the failure of composite. The mechanism of this failure can be explained by the theory developed by Sato et al. (Sato et. al, 1984). Under a tensile load, the stress concentration occurrs in the vicinity of the fibres, especially at the fibre ends. When stress increased, the shear stress increased and it was greatest at the fibre end, as shown in Figure 20. Under the influence of stress concentration and the shear stress, the cracks were resulted at the fibre ends and propagated along the fibre sides, forming interfacial cracks. When the peak stress is reached, the interfacial cracks propagated into the matrix and caused the final composite failure.

3.4.2. Welding Parameters on Strength Development

The butt-joints of PP/30% (w/o) GF-PP were welded according to the techniques described in section 3.3.2 and tested as described in section 3. 3.3. Table 3 records the peak stress of the welded bars of PP/30% (w/o) GF-PP at different welding times and temperatures. The welding pressure was controlled in terms of the displacement by driving the screw bolt. The displacement for welding all the butt-joints is maintained constant by keeping the two parts contact when they were just placed into the weld tool..

Figure 29. is the plot of peak stress of welded PP/30% (w/o) GF-PP bars with various welding times and temperatures by tensile test. From these curves, the time needed to reach a plateau strength of PP/30% (w/o) GF-PP can be determined by the

Table 3: The peak stress of welded joints of PP/30%GFRe-PP with various welding time and temperature

	T_1=167 °C	T_2=170 °C	T_3=174 °C	T_4=180 °C
t_1=30 s	no	no	no	23.5 ± 2.4
t_2=60 s	no	no	no	29.2 ± 0.3
t_3=90 s	no	no	24.7 ± 1.5	31.5 ± 0.4
t_4=120 s	no	16.3 ± 3.7	30.0 ± 1.0	30.4 ± 0.8
t_5=150 s	no	21.2 ± 1.8	29.0 ± 2.0	/
t_6=180 s	15 ± 0.8	26.5 ± 2.8	32.0 ± 0.3	31.3 ± 0.3
t_7=210 s	/	31.5 ± 1.2	/	/
t_8=240 s	23.5±1.4	32.2 ± 1.4	32.9 ± 0.8	/
t_9=270 s	29.8 ± 1.1	/	/	/
t_{10}=300 s	31.5 ± 1.6	30.5 ± 1.6	/	31.3 ± 0.6
t_{11}=360 s	32 ± 1.4	/	/	/
t_{12}=390 s	/	30.4 ± 1.6	/	/
t_{13}=480 s	30.0 ± 1.7	30.4 ± 1.3	31.8 ± 1.3	31.4 ± 0.2

Note:

"no" means no joint at all.
"/" means not available
the unite of peak stress is MPa

Figure 28: SEM micrograph of characteristic failure surface of short GF-PP 30% (w/o) of ASTM tensile test, viewed down on the surface.

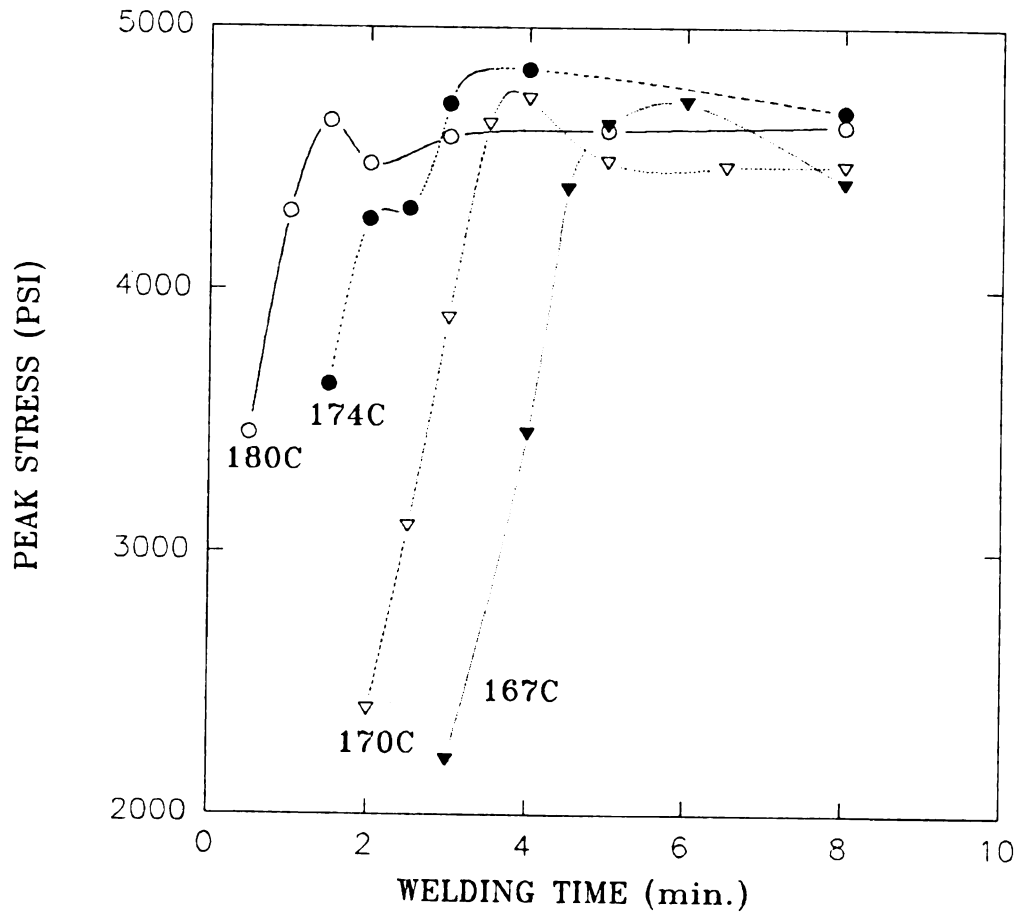

Figure 29: Plot of peak stress of welded PP /30% (w/o) GF-PP bars with various welding times and temperatures by tensile test.

corresponding to the welding temperature. The approximate time for reaching the ultimate strength is about 270 s for 167 ^{o}C, 210 s for 170 ^{o}C, 120 s for 174 ^{o}C and only 60 seconds for 180 ^{o}C. In the experiment, the butt-joint can not be achieved even after 16 minutes, at the welding temperature of 165 ^{o}C, beyond this time, PP will degrade. The higher the welding temperature, the shorter the time for reaching the ultimate strength for a butt-joint. When the welding temperature approaches the melting temperature of the matrix (178 ^{o}C), the time needed to heal the joint is much shorter. This is because the process of healing a polymer joint is more rapid through melting flow than by polymer diffusion alone. These welding parameters can be used to predict the welding of PP and its composites in industry.

The load-displacement curves of welded PP/30% (w/o) GF-PP at 174 ^{o}C for various times under tensile test are illustrated in Figure 30., whereby curve-1, 2, 3, and 4 present the welded bar, welded for 90s, 120s, 240s and 480s, respectively. Although the strength of PP/30%(w/o) GF-PP has reached the ultimate strength when the welding time is longer than 120s at 174 ^{o}C, the elongation of the butt-joints increases with the welding time. From the data in Table 3, the ultimate tensile strength of PP/30% (w/o) GF-PP is about 32 MPa, which is very close to the peak strength of PP, 35 MPa, if the experimental error is taken into consideration. The developed strength of this butt-joint is much lower than that of 30% w/o GF-PP bulk material, 56 MPa. This result is consistent with the study of welding PVDF to it's chopped-graphite-fibre filled PVDF, which has shown that the strength of filled to unfilled material joints could be almost as high as that of the unfilled part (Andrews and Bevis, 1984).

The ultimate strength of a weld bar of PP/30% (w/o) GF-PP is almost the sameas that that of bulk PP. This is not surprising, because when a weak material is jointed to a stronger material, even if the joint is perfect, the strength of such a joint specimen can only reach the strength of the weaker one. The most interesting observation is that failure surfaces of the joint specimens change the appearance with the welding time as well as the

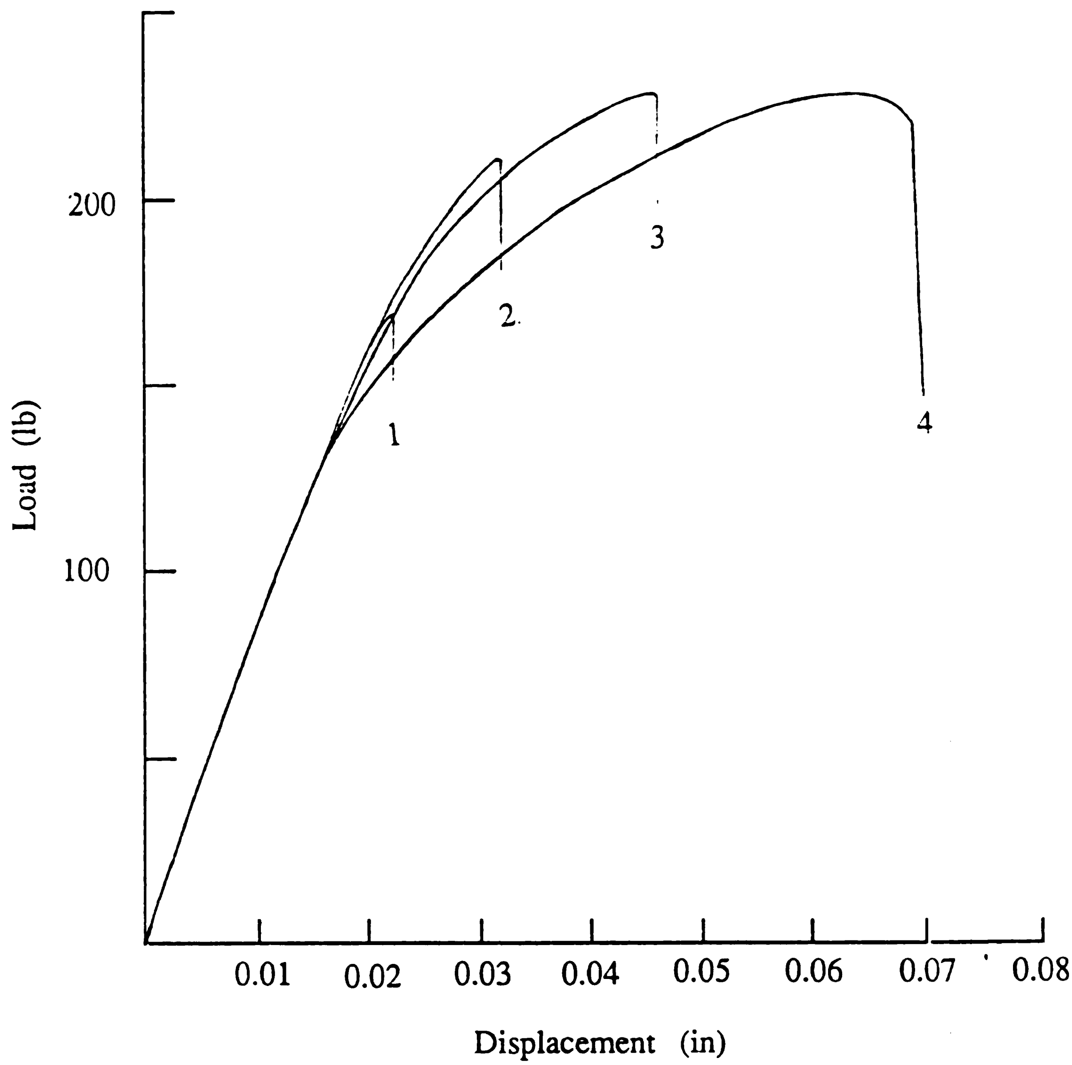

Figure 30: Load-displacement curves for PP/30% GF-PP butt-joints welded at 174 °C for various times by tensile test, curves-1, 2, 3, and 4 represent for 90 s, 120 s, 240 s, and 480 s respectively.

elongation.

Scanning Electron Microscopy inspection of the specimens, after testing, indicated that the failure occurred at or near the weld region (or weld junction), which is related to welding time.

Figure 31. represents the failure surface of PP/30% (w/o) GF-PP welded at 174 ^{o}C for 90 s, (a) at reinforced side: (b) the matched part at PP side; (c) and (d) showing higher magnifications of a small part of (a) and (b) revealing the fibres ends on the surface of reinforced PP and corresponding imprints left on PP side, respectively. From (a) or (b), it is illustrates that the failure of the this butt-joint occurred in the weld surface or junction. The peak strength of this specimen is 24.7 MPa, about 75 percent of the ultimate strength, 32 MPa. The pictures of (c) and (d) show detail of the failure surface at the reinforced and PP sides. The fibres have not protruded outwards into the PP side, and the imprints left on PP side are very shallow and irregular, which indicates that the bond between the fibre ends and matrix did not form in the weld surface, explaining why the strength is lower than the ultimate strength.

When the welding time was increased to 120 s, the peak strength reached the ultimate strength, but most failure area were in the weld junction, as shown in Figure 32., (a) at reinforced side; (b) at PP side. Fig.ure 32. (c) and (d) are viewed at a higher magnification to detail the typical appearance of (a) and (b), respectively. It can be clearly seen the fibres had protruded outwards from reinforced part and into the PP side by the evidence of clearly imprints left in the PP side, as evidenced by the after the failure of joint. However, those outwardly protruding fibres are very short therefore they are most likely located in the same plane which acted as stress concentrators in the whole specimen, under tensile load.

Figure 33 represents the failure surface of PP/30% (w/o) GF-PP welded at 174 ^{o}C for 240 s, (a) at reinforced part; (b) the typical surface appearance on the PP side. The failure surface still coincides with the weld junction, because there are some protruding

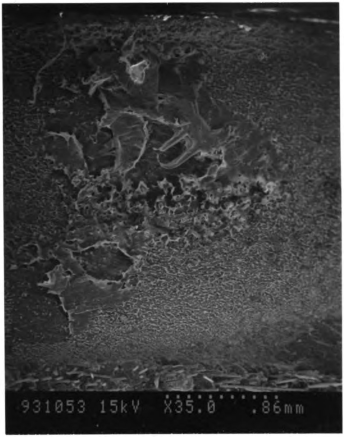

(a)

Figure 31: SEM micrographs of characteristic failure surface of welded PP/30% (w/o) GF-PP at 174 ^{o}C for 90s, (a) at 30% (w/o) GF-PP side.

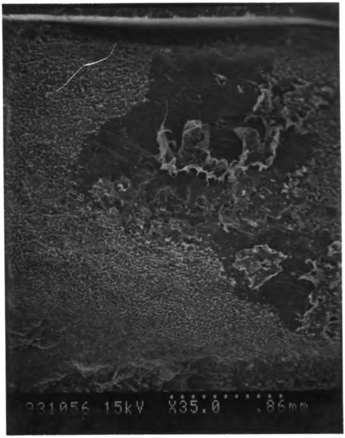

(b)

Figure 31 ---Contd. (b) at PP side

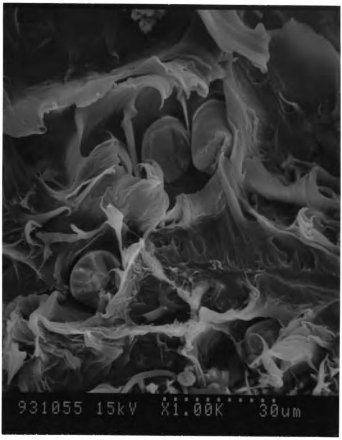

(c)

Figure 31 ---Contd. (c) high magnification SEM micrograph taken from (a)

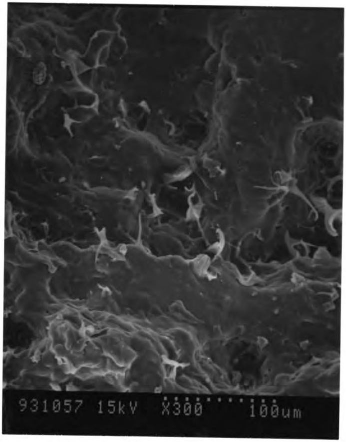

(d)

Figure 31 ---Contd. (d) high magnification SEM micrograph taken from (b)

(a)

Figure 32.: SEM micrographs of characteristic failure surface of welded PP/30% (w/o) GF-PP at 174 ^{o}C for 90s, (a) at 30% (w/o) GF-PP side.

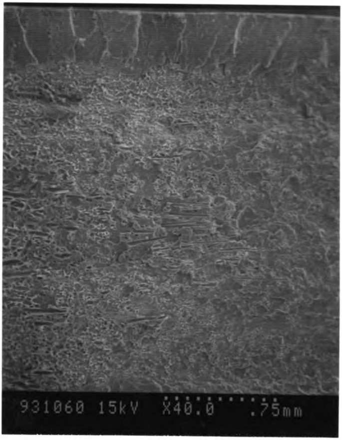

(b)

Figure 32 ---Contd. (b) at PP side

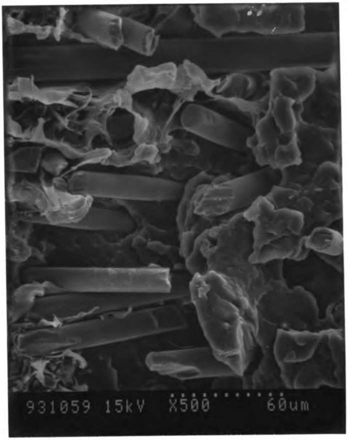

(c)

Figure 32 ----Contd. (c) high magnification SEM micrograph taken from (a)

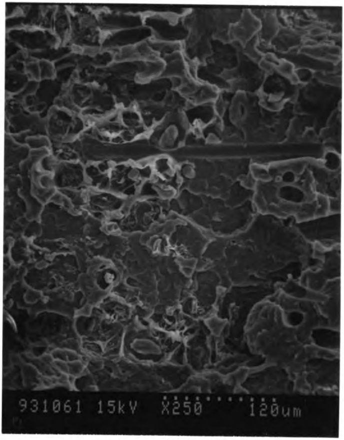

(d)

Figure 32 --- Contd. (d) high magnification SEM micrograph taken from (a)

(a)

Figure 33: SEM micrographs of characteristic failure surface of welded PP/30% (w/o) GF-PP at 174 ^{0}C for 240 s, (a) at 30% (w/o) GF-PP side.

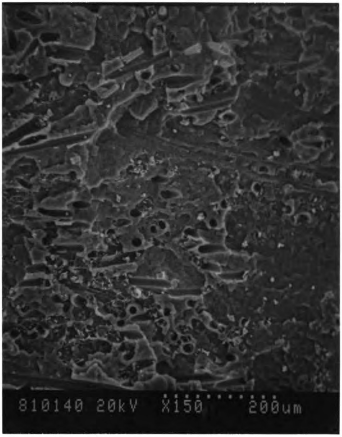

(b)

Figure 33 ---Contd. (b) A typical part at PP side.

fibres on the reinforced part, and correspondingly, some holes and imprints can be observed on the PP side. The obvious difference in Figure 33 as compared to the prior two figures, is the relatively longer of the protruging fibres. The appearance of the failure surface at the reinforced part is obviously different form the failure surface of bulk 30% (w/o) GF-PP tensile specimen, as shown in Figure 28, where the outwardly protruding fibres in the failure plane are much longer, and some resin remaining on them which indicates the reforming bonding in the weld region is better than the specimen welded for shorter time.

When the welding time increases at the same temperature, 174 ^{o}C, most of the failure surface of butt-joint is out of the weld region. Figure 34 is the failure appearance of butt-joint of PP/30% (w/o) GF-PP welded at 174 ^{o}C for 480 s, (a) at reinforced part across the thickness; (b) partial area at the PP part and (c) higher magnification of a small part of (a) to show the detail of transition from ductile to brittle deformation. The whole appearance of the failure surface is convex-concave. There are only some pull-out fibres in the center region which occupy about 8 mm (along the wide of weld bar) in the length and 0.6 mm in width (along thickness), in addition, the deformation of matrix in this region is ductile, but the rest of the area around the center ductile region is brittle failure, and occurred in the PP side. This is known because there is not any debris of fibres can be found, as shown in (a) or (b). In the region of ductile deformation, is the feature of fibril coalescence near the pull-out fibres, which resulted in the rough bundles of deformed matrix. This convex-concave appearance can probably be explained through the layer structure of the injection molded GF-PP, as studied in the last part, and the movement of fibres during the process of welding. The layer structure of the injection molded short GF-PP existed along the thickness, where in the center region, (C), most fibres were arranged longitudially but at both side regions, (S), the fibres were random. In the welding process, due to differing fibre concentrations at both sides (reinforced part 30%(w/o), PP side it is 0%), is different at both sides and the concentration gradient could drive the fibre

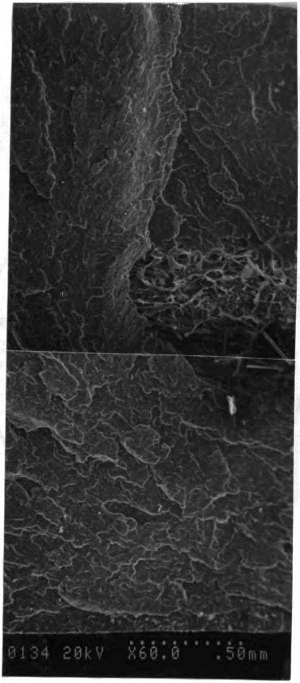

(a)

Figure 34: SEM micrographs of characteristic failure surface of welded PP/30% (w/o) GF-PP at 174 ^{o}C for 480 s, (a) at 30% (w/o) GF-PP side.

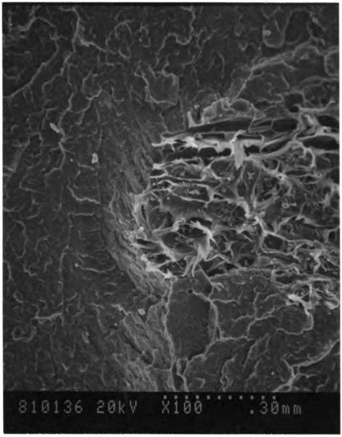

(b)

Figure 34 ---Contd. (b) at PP side

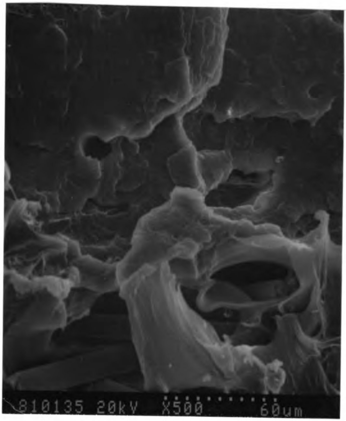

(c)

Figure 34 ----Contd. (c) high magnification SEM micrograph taken from (a)

towards the PP side. The fiber orientation on the weld surface has an important effect on the movement of the fibres, whereby the fibres in the center region are orthonormal to the weld surface and parallel to the movement direction, and therefore, need a lower driving force. However, those fibres in the side regions are random, some lying fibres, perpendicular to the move direction, are difficult to move forwards, or move much more slowly than those fibres in the center. For longer welding times, the fibres in the center region will move longer distances into the PP side, but the fibres at both side regions move very little or stand still at the weld surface. In addition, a longer welding time could benefit for the reformed bonding of fibre/matrix in the weld region.

The differences in failure surface of PP/30% (w/o) GF-PP butt-joints with varying welding times can be better understood with the following explanation . When the welding time is short, but longer enough to reach the ultimate strength of the joint, the fibre ends in the reinforced part lie just at the surface, or just across the junction. Those fibre ends or the lying fibres are concentrated on a single plane -weld junction. When the welded bar is loaded, the crazes will form just below the fibre ends or at fibre sides, as shown in Figure 35 (a) the fribril coalescence near the fibre end and (b) the crazes formed at the left side of the lying fibre and growth to the right along the fibre/matrix interface. Those crazes grow and form microcracks in the weld junction. Due to the high concentration of fibre ends in the single plane, those microcracks approach each other gradually. When they coalesce to some crack size, rapid propagation of the failure will occur in the weld junction, and resulted in a flat surface. However, when the welding time is longer, the fibres in the center region (C) will move a longer distance than those fibres at both side regions, (S), and result in the fibres being found in the center layer bridge in the reinforced part and PP part. Under tensile load, high stress concentration will occur in this area and the cracks form through the fibrils coalescence and broken. When the crack reaches a critical size, the final failure will occur in the PP side instead of the weld junction, because of lower energy through this path, and result in a failure surface with a convex-concave appearance.

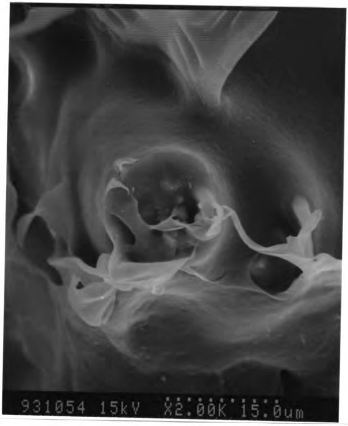

(a)

Figure 35: High magnification SEM micrographs of failure of interfacial bonding reformed in weld region, taken from 174 ^{o}C, 120s. (a) at a fibre end;

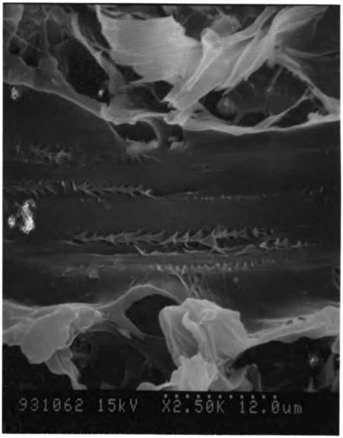

(b)

Figure 35 ---Cont. (b) Inside a imprint after a fiber debonding.

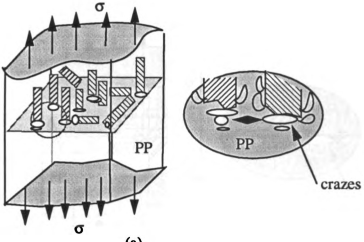

(a)

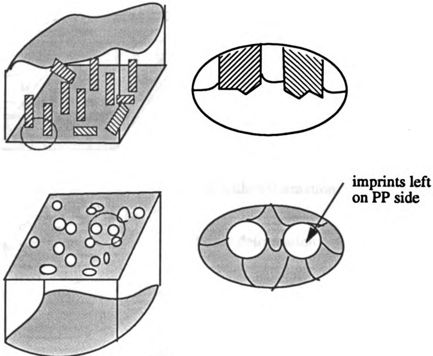

(b)

Figure 36: Schematics for the failure process and surfaces of PP/GF-PP with shorter welding time, (a) under load. crazes forming just under fibre ends; (b) the failure occurring in the weld region.

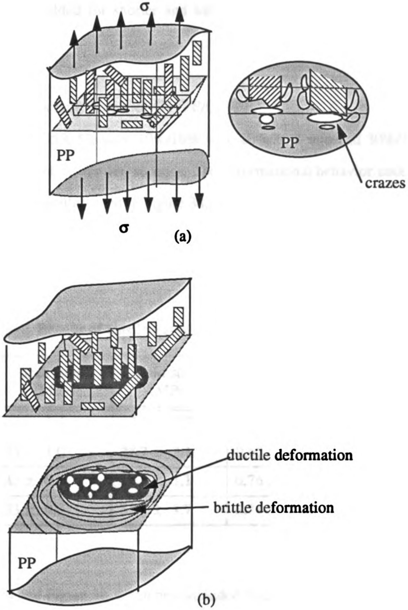

Figure 37: Schematics for the failure of PP/GF-PP with longer welding time, (a) For a longer welding time, the fibres in the center region go further into PP part than fibres in both side regions, crazes forming first in the center region; (b) final failure through PP part and appearance being convex-concave.

The schematic diagrams for the failure processes and failure appearance of PP/30% (w/o) GF-PP, welded for shorter and longer times are shown in Fig. 36. and Fig. 37. respectively.

3.4.3 Tensile Properties Butt-Joints of GF-PP/GF-PP

The butt-joints of 5%/5% w/o, 10%/10% w/o, 20%/20% w/o and 30%/30% w/o GF-PP were welded at 174 ^{o}C for 480 seconds. The deformational behavior under tensile tests of the welded bars are illustrated in Figure 38, which are load-displacement curves of 5%/5%, 10%/10%, 20%/20% and 30%/30% w/o GF-PP from left to right. The results of tensile tests are summarized in Table 4.

Table 4: Results of tensile test of GF-PP/GF-PP butt-joints

type of joints	peak stress (MPa)	yield stress (MPa)	Young's modulus (GPa)	break strain (%)
5%/5% w/o	32 ± 1.4	20.4 ± 0.9	0.58 ± 0.02	16.5 ± 1.3
10%/10% w/o	35 ± 1.0	27.7 ± 2.1	0.65 ± 0.04	10.0 ± 0.7
20%/20% w/o	32 ± 0.3	30.6 ± 1.1	0.76 ± 0.03	8.0 ± 0.6
30%/30% w/o	33 ± 0.8	31.5 ± 1.7	0.71 ± 0.05	7.3 ± 0.4

From Table 4 and Figure 38, it can be concluded that:

(i) the peak strength reached by those butt-joints is almost the same regardless of the fibre content of the two weld parts.

(ii) yield strength and Young's modulus increases with the fibre content of the two weld parts, and the break strain decreases with fibre content.

Visual inspection of the welded butt-joints of GF-PP/GF-PP after tensile testing indicated that all the failure occurred at the weld plane, even for times greater than 480 s, but the mechanical properties were almost the same as those welded for 240s and 480s.

This indicates that the weld region is always the weakest place in the whole butt-joints of GF-PP/GF-PP. For example, Figure 39 represents the failure surface of 30%/30% (w/o) GF-PP welded at 174 ^{o}C for 480s by SEM, (a) at one side failure specimen; and (b) higher magnification of a small part of (a). From (a), it can be observed that the failure occurred in the weld region. The deformation of this surface is dominated by the feature of matrix as compared to the failure surface of 30% (w/o) GF-PP tensile specimen, as shown in Figure 28. In addition, only a few imprints have been left on this surface, which were supposedly to be made by the fibre ends of another part. Those two phenomena might hint to the existance of a thin layer of matrix existed between the two weld surfaces of 30% (w/o) GF-PP, which is possible if taking the polished surfaces of both weld parts into consideration. Most the fibre ends on the polished surface became broken due to polishing, and result in a very uneven surface at the fibre ends as shown in Figure 39 (b). When the two weld surfaces are brought into contact, a gap is formed between any two opposite fibres and provides the space in which a thin layer of matrix can form. In addition, the same fibre content for both weld parts will resist the forward fibre movement and result in fewer fibres penetrating the weld region, and bridging the two parts of the weld specimen. There is also the another reason for the existence of a thin layer of matrix between the two polished surfaces. The existance of a thin layer of matrix in the weld region with very few fibres able to bridge the two parts, are the main reasons for the weld region being the weakest place in the whole specimen of GF-PP/GF-PP, as well as the strength of GF-PP/GF-PP being limited to the strength of bulk PP regardless of the fibre content in the two weld parts. It certainly results the failure occurring in the weld region of any butt-joints of GF-PP/GF-PP.

The failure process of butt-joints of GF-PP/GF-PP can be explained by the following. When the welded specimen is loaded by tensile load, a cluster of crazes will form near the fibre ends in the weld region since this is the weakest place. Those crazes could grow down and up and approach each other in the thin film of matrix in the weld region. They

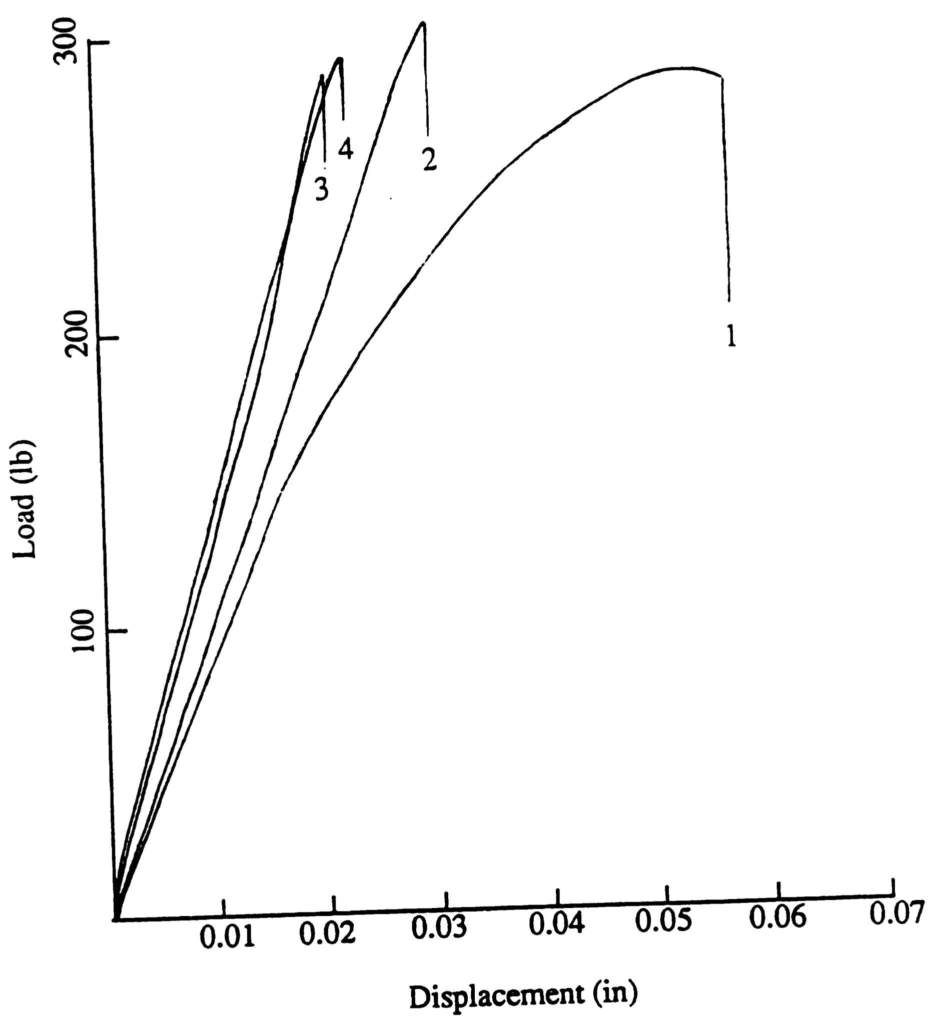

Figure 38: Load-displacement curves for GF-PP/GF-PP butt-joints with various fibre content (w/o) welded at 174 C for 480 s by tensile test: 1 for 5%/5%; 2 for 10%/10%; 3 for 20%/20%; 4 for 30%/30% welded bars.

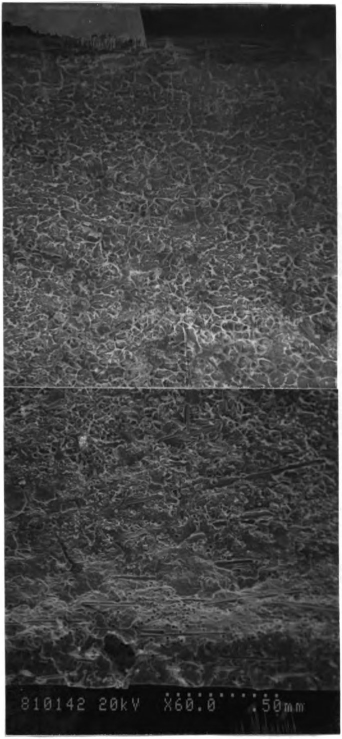

(a)

Figure 39: SEM micrographs of characteristic failure surface of welded 30%/30% (w/o) GF-PP at 174 C for 480 s, (a) at one side of the failed specimen.

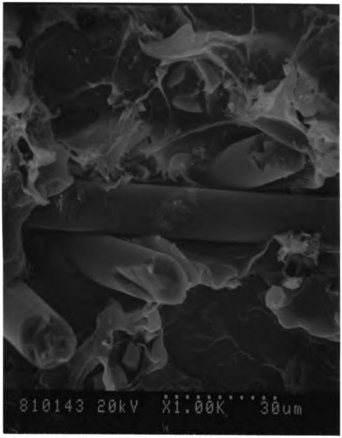

(b)

Figure 39 ---Contd. High magnification SEM micrograph taken from (a).

coalesce and form voids or cracks near the fibre ends, and result in the fibre ends separating from the matrix. When the cracks reach a critical size, the brittle failure occurs in the weld region and causes the final failure of the whole specimen. All of these failure processes are illustrated schematically by Figure 40, (a) butt-joint of GF-PP/GF-PP; (b) crazes forming at the fibre ends in the weld region; and (c) cracks propagating in the thin layer of matrix, resulting the final failure of the joint in the weld region.

Unlike the strength of GF-PP/GF-PP being limited to the strength of bulk PP, the yield strength and modulus increase with the fibre content in the two weld parts, as recorded in Table 4. Both of them are not only relative with the properties of the weld region, but also relative with the properties of the both sides. The both side of weld region are bulk reinforced PP, which are much stiffer than the material in the weld region because there are no effectively reinforced fibres and a thin layer of matrix exists in the weld region. The deformation will occur in the weld region first under loading and then restricted in this region by both sides. The higher the fibre content in the two weld parts, the stronger the restriction of the both sides acting upon the welding region. However, as the difference between the property of the weld region and the weld parts at both sides becomes greater and greater, the property of weld region will have more important effect on the whole butt-joint. This is why the yield strength and modulus of the butt-joints of GF-PP/GF-PP increase with fibre content in GF-PP from 5% to 20% (w/o), but do not change much from 20% to 30% (w/o), as shown in Table 4. On the other hand, the break strain of this kind of joint will decrease with the fibre content in the two weld parts.

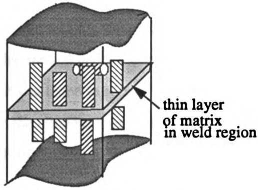

(a) butt-joint of GF-PP/GF-PP

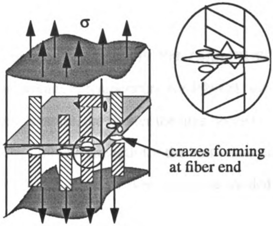

(b) under stress, crazes form near fiber ends and growth

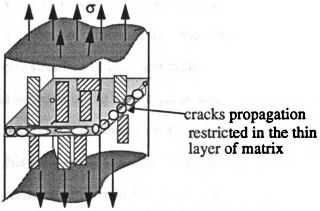

(c) crazes coalescence to forming cracks and propagation in the thin layer of matrix and result the final failure in the weld region

Figure 40: Schematics of the failure processes of GF-PP/GF-PP.

3.5 Summary

A systematic study of the butt-joints of PP to short GF-PP and GF-PP to GF-PP has been carried out.

The welding time required to reach the ultimate strength of PP/ 30% (w/o) FG-PP was determined under various temperatures. The minimum temperature for PP/30% w/o GF-PP was found to be 167 ^{o}C. The higher the temperature, the shorter the time needed to obtain the ultimate strength for the butt-joints. The ultimate strength for the butt-joints of PP/GF-PP is close to the peak strength of bulk PP, which is the weaker one in the welded bar.

The failure appearance of PP/GF-PP is affected by the welding time, even after the ultimate strength has been reached. For a shorter welding time, the failure place always coincides with the welding surface, owing to most of the fiber ends and lying fibers from the reinforced parts being located on a single plane. For a longer welding time, the failure starts at the center area of the weld region with final failure through the PP part, resulting in a convex-concave appearance. This is because most of the fibers in the center region are arranged along the injection direction, and the fibers at both side regions are random according to the layer structure of injection molded GF-PP. The fibers in the center region can move easier than those in the side regions and are able to move further into the PP part. The stress concentration occurs near those fiber ends and generates cracks through crazes forming at this area, then causes the final failure in the PP side.

The reinforcement of fiber in PP is cancelled out by introducing a weld into the system of GF-PP/GF-PP. The peak strength this joint can reach limited to that of bulk PP, because there are very few fibers able to penetrate the weld plane and bridge two weld parts, with a thin layer of matrix existing in the weld region. Owing to the different properties between the weld region and the two weld parts, the stiffer material at both sides of weld region will restrict the occurrence of deformation and propagation in the weld region, and the failure of the butt-joint of GF-PP/GF-PP will result at the weld region, which is the weakest place in the whole bar.

CHAPTER 4

CONCLUSIONS

The increment of fracture toughness, Kc, is dependent upon the fiber content at low temperature. When fiber content is low (from 5% to 10% w/o), Kc increases quickly and the mechanism of toughening can be explained by crack pinning. The fracture toughness increases much slower when fiber content is above 10% (w/o) and in this case, crack deflection is best to be used to explain the toughening mechanism. In addition, other energy consuming mechanisms intervene during crack propagation and exist simultaneously, such as fiber pull-out, plastic deformation of matrix (homogeneously and localized), debonding of the fiber-matrix interfaces and a few broken fibers.

Under current testing conditions, crazing provides a mechanism for absorping and dissipation of fracture energy for a notched specimen of PP.

It was found that the CT specimen with the T-notch had a higher value of fracture toughness than that with the L-notch for the same fiber content. This is because more fibers were arranged transverse to the prenotch in the T-notch specimen than that in the L-notch specimen, according to the layer structure of injection molded GF-PP.

The second part investigated the butt-joint of PP to short GF-PP and GF-PP to itself.

The welding parameters of time and temperature on the strength development of PP/GF-PP was carried out and it was found that the higher the temperature, the shorter the time needed to obtain the ultimate strength for the butt-joint. The minimum temperature for PP/30% w/o GF-PP is found to be 167 ^{o}C. The ultimate strength for the butt-joints of PP/GF-PP is close to the peak strength of bulk PP, which is the weaker part one in the welded bar.

The failure appearance of PP/GF-PP was found to be effected by the welding time, even after the ultimate strength has been reached. For a shorter welding time, the failure occurred in the weld region, owing to most of the fiber ends and lying fibers from the reinforced parts being located on a single plane. For a longer welding time, the failure starts at the center region of the weld region, then final failure through the PP part, and results in a convex-concave appearance. This is because most of the fibers in the center region are arranged along the injection direction and the fibres at both side regions are random according to the layer structure of the injection molded GF-PP. The fibers in the center region can move easier than those in the side regions and move further into the PP part in a relatively longer time. The stress concentration occurs near those fiber ends and generate cracks through the formation crazes of at this area and then cause the final failure in the PP side.

The reinforcement of fiber in PP is cancelled out by introducing a weld into the system of GF-PP/GF-PP. The strength that this joint can reach is limited to that of bulk PP since there are very few fibers able to penetrate the weld plane and bridge two weld parts, with a thin layer of matrix existing in the weld region. There is the main reason for the reductional properties of the butt-joints of GF-PP/GF-PP. The reinforced PP at both sides of weld region is stiffer, restricting the deformation in the weld region, and the failure place of the butt-joint of GF-PP/GF-PP will result at the weld region, which is the weakest place in the whole bar.

BIBLIOGRAPHY

Gupta, V.B., Mittal, R.K., and Goel, Malti: *Compos. Sci. Technol.* **37** 353 (1991)

Friedrich, K. and Karger-Kocsis, J.: *Fractography and Failure Mechanisms of Polymers and Composites*, Elsevier Science Publishers LTD, London and New York, 437-494 (1989)

Lange, F. F.: *Phil. Mag.* **22** 938 (1970)

Lange, F. F. and Radford, K. C.: *J. Mater. Sci.* **6** 1197 (1971)

Evans, A. G.: *Phil. Mag.* **26** 1327 (1972)

Kinloch, A. J., Maxwell, D. A. and Young, R. J.: *J. Mater. Sci. Lett.* **4** 1276 (1987)

Cantwell W. J. and Anne C. Roulin-Moloney: *Fractography and Failure Mechanisms of Polymers and Composites*, edited by Anne C. Roulin-Moloney, Elsevier applied Science, London and New York, 233-290 (1989)

Binns, D. B.: *Science of Ceramics*, edited by Steward, G.H., Academic Press, New York, 315 (1962)

Faber, K. T. and Evans, A. G.: *Acta Metall.* **31** 565 (1983)

Owen, A. B.: *J. Mater. Sci.* **14** 2523 (1979)

Lin, G. M. and Lai, J. K. L.: *J. Mater. Sci.* **28** 5240 (1993)

Griffth, A. A.: *Phil. Trans. Roy. Soc.* **221** 163 (1921)

Turner, S.: *Mechnical testing of Plastic*, 2nd edition, (1983)

Fraser, R. A. W. and Ward, I. M.: *J. Mater. Sci.*, **12** 459 (1977),

Baneal P. P. and Ardell, A. J.: *Metallography*, **5** 92 (1972)

Kausch, H. H.: *Polymer Fracture*, Berlin-Heidelberg-New York springer, (1978)

Hannon, M.J.: *J. Appl. Polym. Sci.* **18** 3761 (1974)

Kitagawa, M. and Yammaura, H.: *J. Mater. Sci.* **19** 1863-1875 (1984)

Jud, K., Kausch, H. H., and Williams, J. G.: *J. Mater. Sci.* **16** 204 (1981) de Gennes, P. G. de: *J. Chem. Phys.* **55** 572 (1971)

Wool, R. P. and O'Connor, K. M.: *J. Polym. Sci. Polym.* Letters Ed., (1981)

Wool, R. P. and O'Connor, K. M.: *J. Poly. Sci.*, **20** 7 (1982)

Kim, Y. H. and Wool, R. P.: *Macromolecules*, **16** 115 (1983)

Prager, S., Adolf, D. and Tirrell., M.: *J. Chem. Phys.* **78** 7105 (1983)

Storkes, V. K.: *Polym. Eng. Sci.* **28** 728 (1988)

Strokes, V. K.: *Polym. Eng. Sci.*: **31** 511 (1991)

Battien L.J. and Gillespie, J. W. JR.: *Polym. Eng. Sci.*, **31** 1720 (1991)

Andrews, J.R.F. and Bevis, M.J. J.: *Mater. Sci.* **19** 645 (1984)

Cox, H. L.: *J. Appy. Phys.*: **3** 72 (1952)

Brady, T. E., Yeh, G. S. Y.: *J. Mater. Sci.*, **5** 573 (1970)

Olf,H.G. A., Peterlin, H.G.A.: *J. Polym. Sci., Polym. Phys.* **12** 2209 (1974)

Friedrich, K.: *Advanced in Polymer Science*, Vol. **52/53** (1983)

Sato, N., Kurauchi, T., Sato, S. and Kamigaito, O.: *J. Mater. Sci.*, **19** 1145 (1984)

Voyutskii, S. S.: *Autohesion and Adhesion of High Polymers*, Wiley-interscience, New York, (1963)

Jud, K. and Kaush, H. H. : *Polymer Bull.* **1** 697 (1979)